行政院國家科學委員會補助

大專學生參與專題研究計畫研究成果報告

＊ ********* ** ＊
＊ 計 畫 ＊
＊ ： 熱壓密問題之數學模式的建立與解析 ＊
＊ 名 稱 ＊
＊ ********* ** ＊

執行計畫學生： 梁惠娟
學生計畫編號： NSC 98-2815-C-216-007-E
研 究 期 間 ： 98 年 07 月 01 日至 99 年 02 月 28 日止，計 8 個月
指 導 教 授 ： 呂志宗

處理方式： 本計畫可公開查詢

執 行 單 位： 中華大學土木與工程資訊學系

中華民國 99 年 03 月 31 日

行政院國家科學委員會補助

大專學生參與專題研究計畫研究成果報告

＊＊＊＊＊＊＊＊＊＊＊＊＊＊＊＊＊＊＊＊＊＊＊＊＊＊＊＊＊＊＊＊＊＊＊＊
＊ 計畫 ＊
＊ ： **熱壓密問題之數學模式的建立與解析** ＊
＊ 名稱 ＊
＊＊＊＊＊＊＊＊＊＊＊＊＊＊＊＊＊＊＊＊＊＊＊＊＊＊＊＊＊＊＊＊＊＊＊＊

執行計畫學生：梁 惠 娟

學生計畫編號：NSC 98-2815-C-216-007-E

研 究 期 間 ：98 年 7 月 1 日至 99 年 2 月底止，計 8 個月

指 導 教 授 ：呂 志 宗

執 行 單 位：中華大學土木與工程資訊學系

中華民國 九十九 年 三 月 三十一 日

摘　　要

本計畫之研究重點有三個，包括：(1)多孔介質三維熱壓密理論的研討與整理，(2)點熱源所引致熱壓密問題之數學模式的建立，(3)以積分轉換方法配合數值分析技巧解析出熱壓密問題的解析解。本計畫已蒐集、分析並整理出以 Biot 多孔介質彈力理論為基礎之三維熱壓密理論的各種不同類型，然後引用合適之自然律與時空條件，建立符合點熱源作用情況下之數學模式，其中地層可分別模擬為均質之等向性或橫向等向性的線彈性飽和多孔介質，孔隙水的流動需遵守 Darcy 定律與質量守恆定律，熱量的流動需遵守 Fourier 熱傳導定律與能量守恆定律，固體介質之變形則需服從牛頓第二運動定律與虎克定律等。本研究係以積分轉換等方法，研討出點熱源所引致的地層位移、有效應力、溫度變化量與超額孔隙水壓變化量等，研究成果應有助於工程上之相關應用。根據本研究之探討得知以下重要研究成果。

由 3-2 單元之研究結果得知：(1)在「穩定熱源」作用的考量下，隨著熱源作用時間的增加，地層中各點之溫度會逐漸上升，最後形成一穩態平衡。(2)在「瞬時熱源」作用的考量下，隨著熱源作用時間的增加，地層中各點之溫度會先上升然後逐漸下降，最後上升之地層溫度會完全消失。

由 3-3 單元之解析結果得知：(1)地層中所有的熱彈性行為均與觀察點至熱源的距離有關，且與地層之線性熱膨脹係數成正比，但與地層之熱傳導係數成反比；另外，由研究結果得知，地層之溫度變化及位移變化均與地層剪力模數無關。(2)地層之橫向等向性特徵對地層之熱應力有明顯的影響，例如當線性熱膨脹係數比 α_{sr}/α_{sz} 增加時，所引致之熱應力會明顯上升；但線性熱傳導係數比 $\lambda_{tr}/\lambda_{tz}$ 增加時，所引致之熱應力會明顯下降。(3)在等向性地層的考慮下，徑向正向熱應力 σ_{rr} 與垂直正向熱應力 σ_{zz} 之比值介於 0.5~2.0，而環向正向熱應力 $\sigma_{\theta\theta}$ 與垂直正向熱應力 σ_{zz} 之比值則介於 0.5~1.0。

由 3-4 單元之研討結果得知：(1)引用熱彈性力學與多孔介質彈力理論之類比關係，瞬時熱源所引致之地層熱彈性行為可轉換為瞬時抽水問題的解。(2)瞬時熱源作用於地層時，地層之各項熱彈性反應會在一瞬間達到極大值，然後再逐漸消散，因將地層模擬為彈性介質，故各種地層之熱彈性行為變化最後都會完全消失。(3)地表因瞬時熱源作用所引致之最大水平位移約為最大垂直位移的 38.5%，顯然瞬時熱源作用時，所引起的地表水平位移是不宜忽略的。

關鍵詞：點熱源，熱壓密，解析解，積分轉換法，多孔介質，半無限域

目　　錄

第一章　緒　　論

1-1　研究主旨

熱對地層力學行為影響之研究係土木工程中之重要研究主題。熱發生之原因甚多，例如：地球內部釋放出之高溫地熱所引致，氣候變化引起地層溫度改變，冰凍施工方法使土層溫度發生變化，垃圾掩埋場因廢棄物分解產生熱能等。近來，有關核廢料埋置於深層地層時，輻射熱對地層穩定性之研討，亦廣受重視。由於埋置地層會因核廢料之輻射熱所產生之高溫而影響其穩定性，為確保存放地點安全可靠，有必要對熱源所引致之地層力學行為詳加研討。

土壤的壓密理論發展甚早，早期之研究多偏重於探討地表荷重所引致之壓密。在陸續的研究中，有關抽取地下水所引致之地盤壓密沉陷亦曾被廣泛研討。近來，熱在地層中擴散傳播所引致之地層力學行為變化則受到重視。當地層受熱影響時，由於孔隙水因溫度身高所引致之體積膨脹量較固體土粒為大，因此，熱源作用之初期階段，將導致孔隙水壓力升高，升高之孔隙水壓力則因孔隙水滲透而逐漸消散，致使土層發生壓密現象，稱之為熱壓密（thermo-consolidation）。

熱壓密理論與多孔介質（porous medium）有關，在與擴散傳播等現象有關之問題上均有應用，於是多孔介質彈性力學理論（poroelasticity）逐漸發展，而受重視。基於此，本文旨在研討熱與孔隙流體在多孔介質中擴散傳播之機制，建立多孔介質熱彈性力學理論，據以探討熱影響之三維壓密問題。

基於所研討出之熱壓密理論，本研究分別探討深層暨淺層熱源影響之壓密問題。數學模式中，模擬地層為均質且等向性之飽和線彈性多孔介質，分別建立耦合、部分耦合與非耦合等三維熱壓密之數學模式，並加以研討、比較。以積分變換方法（integral transform）解析數學模式，推導出與時間有關之閉合解（closed-form solution），並圖示其與土壤參數間之關係，使有助於了解熱壓密問題。

有關地表邊界影響之熱壓密亦將加以研究。數學模擬中，係將地表模擬為一平面，延伸至無限遠處。以地表面下之一穩定熱點源模擬為熱作用源，利用積分變換方法解析數學模式，推導出與時間有關之熱壓密閉合解。以上之研究，可做為進一步研討熱壓密問題之基礎。

1-2　有關研究之回顧

Terzaghi[1]首先提出簡化之單向度壓密理論，用以解析大地工程中，受地表荷重影響之土壤壓密問題後，相關之研究，不勝枚舉。Biot[2]則建立三維之耦合壓密模式，並推展至異向性介質[3]。一般公認，Biot[2,3]壓密模式較嚴謹合理，

而廣受重視。為使 Biot 壓密理論中所定義之力學常數易於以試驗獲得，Corapcioglu 與 Bear[4]、Verruijt[5]、Rice 與 Cleary[6]等曾定義新的工程常數，將 Biot 壓密模式重新改寫，以利於應用。Biot[2,3]、Rice 與 Cleary[6]所建立之壓密模式係考慮孔隙水與固體介質均可壓縮；另一由 Verruijt[5]、Corapcioglu 與 Bear[4]所建立之壓密模式，僅考慮孔隙水可壓縮，而固體介質則模擬為不可壓縮，以上壓密模式均為研討熱效應的影響。

在陸續的研究中，基於 Biot[2,3]壓密理論，Schiffman[7]建立三維熱彈性壓密模式；Bear 與 Corapcioglu[8]曾研討於含水層（aquifer）中，抽取（或補注）高溫或低溫地下水時，含水層之熱彈性壓密數學模式，但並未加以解析。Aboustit 等人[9]、Geraminegad 和 Saxena[10]等對平面應變下，熱彈性壓密之有限元素法解析做過研究。基於 Rice 與 Cleary[6]所建立之 Biot 壓密模式，McTigue[11]曾探討飽和多孔介質中，熱影響之壓密模式並加以解析。Booker 與 Savvidou[12-14]模擬地層為均質等向性或異向性之線彈性多孔介質，研討單點熱源[12]與熱球體熱源[13]引致之壓密，並探討異向性滲流情況下之熱壓密[14]。Booker 等人[12-14]所建立之熱壓密模式，係考慮熱傳導僅與土壤溫度變化有關。

溫度變化對地層力學行為變化的影響，係土木工程等相關領域中之重要研究主題[15]，長久以來即廣受各界關注。有關地層溫度發生變化的原因甚多，例如補注高溫或低溫之地下水[16]、氣候變化[17]或冰凍工法[18]等會使地層溫度發生改變，而地球內部所釋放出之高溫地熱[19]、垃圾掩埋場因廢棄物分解致產生熱能[20]等，亦為重要影響因素。近來，有關核廢料桶埋設於深層地層時，輻射熱對地層穩定性影響之探討，亦廣受重視[21,22]，若埋設地層不穩定或掩埋場址設計不當，便極可能因核廢料桶所釋放出之高溫而影響地層穩定性。為確保存放地點安全可靠，避免輻射物質污染地下水層或生物圈，故有必要對熱作用源所引致之地層力學行為變化詳加研討。

Lu 與 Lin[23-25]曾探討地表邊界對單點熱源所引致之暫態熱壓密現象的影響；Lu[26]亦曾探討深層點熱源對橫向等向性地層之熱壓密的影響。Ma 和 Hueckel[22]對於埋置在粘土地層中之高溫核廢料所引起的土層應力及孔隙水壓力變化等，亦曾作過數值模擬研究。Edgar、Nelson 和 McWhorter[27]基於 Terzaghi[1]壓密模式，曾探討不飽和土壤的熱壓密問題。Britto 等人[28]曾以試驗及有限元素之數值模擬方法解析圓柱形狀熱源引致之壓密；Seneviratne、Carter 與 Booker 等人[29]亦曾引用有限元素法解析圓柱形狀熱源引致之壓密。這一類問題的研討與解析，直到如今仍廣受各界的重視[30-41]。

1-3 本計畫報告內容與組織

本計畫報告共分三章，簡要說明如下：

第一章為緒論，簡述熱壓密問題之背景與研究動機，說明因熱所引致的地層壓密問題之相關研究。

第二章為三維熱壓密理論之研討，基於三維壓密理論與熱彈性力學理論，研

討熱與孔隙流體在多孔介質中之擴散傳輸模式，建立耦合、部分耦合與非耦合之三維熱壓密理論。

第三章係研討深層暨淺層熱源引致之壓密問題。研討出熱源影響之土壤位移、熱應力與溫度變化等之解析解，並研討各項土壤參數對不同熱壓密模式的影響。有關地表邊界受熱源影響之壓密問題亦加研討。基於非耦合三維壓密理論，模擬土壤為一半無限域，以積分變換方法解析數學模式，推導出受單點瞬時熱源影響時，地表面之位移解析解。以上研討結果可作為進一步探討熱壓密問題之基礎。

第二章　熱壓密理論

2-1　能量平衡原理

熱壓密理論與熱及孔隙流體在多孔介質中之擴散傳輸有關。本章基於Nowacki[42]所建立之熱彈力學理論與 Biot[2,3]所建立之耦合三維壓密理論，研討多孔介質熱彈性力學模式，以作為研究熱壓密問題之基礎。

茲考慮以下之基本假設：

1. 微小應變理論適用。
2. 介質之溫度變化量θ滿足$|\theta/T_0|<<1$之條件，其中$\theta=T-T_0$，T與T_0分別表介質受熱後之溫度與其初始溫度。
3. 所分析之代表性多孔介質元素中之固體介質與孔隙流體的溫度相同。
4. 忽略因溫度升高使孔隙流體上浮所引致之自然熱對流（natural convection）現象。

基於此，則多孔介質中之應變位移的線性關係式可表為：

$$\varepsilon_{ij}=\frac{1}{2}\left(u_{i,j}+u_{j,i}\right)，\tag{2.1a}$$

$$\in_{ij}=\frac{1}{2}\left(v_{i,j}+v_{j,i}\right)，\tag{2.1b}$$

式中u_i與v_i分別表固體介質與孔隙流體之位移；ε_{ij}與$\in_{ij}$分別為固體介質與孔隙流體之應變，此應變須分別滿足應變相容條件，即：

$$\varepsilon_{ij,kl}+\varepsilon_{kl,il}-\varepsilon_{ik,jl}-\varepsilon_{il,ik}=0，\tag{2.2a}$$

$$\in_{ij,kl}+\in_{kl,ij}-\in_{ik,jl}-\in_{jl,ik}=0。\tag{2.2b}$$

由熱力學第一定律知，熱量的擴散傳輸需遵循能量平衡原理，亦即：

$$\dot{L}+\dot{Q}=\dot{U}+\dot{K}，\tag{2.3}$$

式中$\dot{L}$表外力作用於多孔介質所引致之功率（power）；$\dot{Q}$表單位時間內多孔介質

所增加之熱量；$\dot{U}$ 與 $\dot{K}$ 分別表儲存於介質中之內能與動能的增率。

作用於飽和多孔介質上之外力包括徹體力與表面應力，因此，外力作用所引致之功率 $\dot{L}$ 可表為:

$$\dot{L}=\int_A T_i^s \dot{u}_i dA+\int_V (1-n)x_i^s \dot{u}_i dV+\int_A T_i^f \dot{v}_i dA+\int_V nx_i^f \dot{v}_i dV \text{，} \tag{2.4}$$

式中 n 為介質之孔隙率（porosity）；x_i^s 與 x_i^f 分別為固體介質與孔隙流體之徹體力；T_i^s 與 T_i^f 分別表作用於固體介質與孔隙流體之表面應力，且 $T_i^s=(1-n)T_i$，$T_i^f=nT_i$，T_i 係作用於多孔介質之總表面應力。基於此，將式(2.4)改寫為：

$$\dot{L}=\int_A (1-n)T_i \dot{u}_i dA+\int_V (1-n)x_i^s \dot{u}_i dV+\int_A nT_i \dot{v}_i dA+\int_V nx_i^f \dot{v}_i dV \text{。} \tag{2.5}$$

茲引用 Cauchy 公式，將作用於邊界上之應力表為：

$$T_i^s=\sigma_{ij}n_j \text{，} T_i^f=\sigma n_i \text{，} \tag{2.6}$$

其中 n_i 係多孔介質在邊界上之單位法線向量（unit normal vector，向外為正）。由牛頓第二運動定律知，作用於固體介質面積上之應力 σ_{ij} 與作用孔隙流體面積上之應力 σ 均須滿足力平衡方程式，亦即：

$$\sigma_{ij,j}+(1-n)x_i^s=(1-n)\rho_s \frac{d\dot{u}_i}{dt} \text{，} \tag{2.7a}$$

$$\sigma_{,i}+nx_i^f=n\rho_f \frac{D\dot{v}_i}{Dt} \text{，} \tag{2.7b}$$

式中 $\frac{D}{Dt}=\frac{\partial}{\partial t}+(\dot{u}_i-\dot{v}_i)\frac{\partial}{\partial x_i}$；$\frac{d}{dt}=\frac{\partial}{\partial t}+\dot{u}_i\frac{\partial}{\partial x_i}$；$\rho_s$ 與 ρ_f 分別為固體介質與孔隙流體之密度；x_i^s 與 x_i^f 分別為固體介質與孔隙流體之徹體力（body force）。由 Terzaghi[1] 的有效應力觀念知：

$$\tau_{ij}=\sigma_{ij}+\sigma\delta_{ij} \text{，} \tag{2.8}$$

其中 τ_{ij} 表作用於多孔介質上之總應力，且

$\sigma = -np$ ， (2.9)

式中 p（壓力為正）表超額孔隙流體壓力（excess pore fluid pressure），係流體之錶測壓力（gauge pressure）變化量。

其次引用 Gauss 定理與力平衡關係式(2.7)，將式(2.4)中之面積分項改寫為體積分，則外力作用於多孔介質所引致之功率 $\dot{L}$ 可表為：

$$\dot{L} = \int_V \left\{ (1-n)\rho_s \frac{d\dot{u}_i}{dt}\dot{u}_i + \sigma_{ij}\dot{u}_{i,j} \right\} dV + \int_V \left\{ n\rho_f \frac{D\dot{v}_i}{Dt}\dot{v}_i + \sigma\dot{v}_{i,i} \right\} dV 。 \quad (2.10)$$

茲考慮多孔介質內部熱量增加之原因包括:

1. 熱量由高溫區流向低溫區時，藉由熱傳導作用所引致之介質內部的熱量增加。
2. 藉由孔隙流體流動，將熱量輸入介質內部之強制熱對流（forced convection）作用。
3. 介質內部之熱源所產生之熱量。

基於此，考慮固體介質與孔隙流體間之相對位移，則多孔介質內部之熱量增率 $\dot{Q}$ 可表為:

$$\dot{Q} = -\int_A q_i n_i dA + \int_A n\rho_f c_{vf}\theta(\dot{v}_i - \dot{u}_i) n_i dA + \int_V W dV ， \quad (2.11)$$

式中 q_i 為熱量流率（heat flux）; c_{vf} 表孔隙流體在固定應變下所測得之比熱; W 係單位時間單位多孔介質體積內所產生之熱量。

由質量平衡（mass balance）定理知：

$$\frac{d\rho}{dt} + \rho\dot{\varepsilon} = -\left[n\rho_f (\dot{v}_i - \dot{u}_i) \right]_{,i} ， \quad (2.12)$$

其中 ρ 表多孔介質之密度， $\rho = (1-n)\rho_s + n\rho_f$ ， $\varepsilon = u_{i,i}$ ， $d/dt = \partial/\partial t + \dot{u}_i \partial/\partial x_i$ 。若流體之密度無顯著變化，則流體之密度 ρ_f 可考慮為常數。一般固體介質之壓縮性甚小，因此 $\dot{\varepsilon} = \dot{u}_{i,i} = 0$ 。基於此，式(2.12)可改寫為：

$$\left[n\rho_f (\dot{v}_i - \dot{u}_i) \right]_{,i} = 0 。 \quad (2.13)$$

以此為基礎，並引用 Gauss 定理與式(2.13)，將式(2.11)中之面積分項改寫為體積分，則多孔介質內部之熱量增率為：

$$\dot{Q} = -\int_V \left[q_{i,i} - n\rho_f c_{vf} \theta_{,i} \left(\dot{v}_i - \dot{u}_i \right) - W \right] dV \text{ 。} \tag{2.14}$$

式(2.3)中之U係表儲存於多孔介質中之內能，令自由能（free energy）U^*表在單位多孔介質體積內所儲存之內能，則：

$$\dot{U} = -\int_V \dot{U}^* dV \text{ 。} \tag{2.15}$$

有關介質內部動能之增率$\dot{K}$可表為：

$$\dot{K} = -\int_V \left[\left(1-n\right) \rho_s \frac{d\dot{u}_i}{dt} \dot{u}_i + n\rho_f \frac{D\dot{v}_i}{Dt} \dot{v}_i \right] dV \text{ 。} \tag{2.16}$$

茲將式(2.10)、式(2.14)、式(2.15)與式(2.16)代入式(2.3)中，並作適當之化簡，則可得能量平衡方程式如下所式：

$$\int_V \left[\dot{U}^* - \sigma_{ij} \dot{u}_{i,j} - \sigma \dot{v}_{i,i} + q_{i,i} - n\rho_f c_{vf} \theta_{,i} \left(\dot{v}_i - \dot{u}_i \right) - W \right] dV = 0 \text{ 。} \tag{2.17}$$

由式(2.17)得知，單位多孔介質體積中之內能增率為：

$$\dot{U}^* = \sigma_{ij} \dot{u}_{i,j} + \sigma \dot{v}_{i,i} - q_{i,i} + n\rho_f c_{vf} \theta_{,i} \left(\dot{v}_i - \dot{u}_i \right) + W \text{ 。} \tag{2.18}$$

由微小應變理論知：

$$\dot{u}_{i,j} = \frac{1}{2}\left(\dot{u}_{i,j} + \dot{u}_{j,i} \right) + \frac{1}{2}\left(\dot{u}_{i,j} - \dot{u}_{j,i} \right) = \dot{\varepsilon}_{ij} + \dot{\omega}_{ij} \text{ ，} \tag{2.19}$$

其中ω_{ij}表固體介質之旋轉張量（rotation tensor）。茲因作用於固體介質上之應力σ_{ij}具對稱性，ω_{ij}則具反對稱性（skew-symmetric），即$\omega_{ij} = -\omega_{ji}$，因此$\sigma_{ij}\dot{\omega}_{ij} = 0$。所以，式(2.18)可改寫為：

$$\dot{U}^* = \sigma_{ij}\dot{\varepsilon}_{ij} + \sigma \dot{\in} - q_{i,i} + n\rho_f c_{vf}\theta_{,i}\left(\dot{v}_i - \dot{u}_i\right) + W \text{ ，} \tag{2.20}$$

其中$\in = v_{i,i}$。

熱在多孔介質中之傳輸亦應遵循熱力學第二定律。由熵平衡（entropy balance）定理知：

$$T\dot{S}^* = -q_{i,i} + n\rho_f c_{vf}\theta_{,i}\left(\dot{v}_i - \dot{u}_i\right) + W \text{ ，} \tag{2.21}$$

其中S^*表單位多孔介質體積內因熱量變化所引致之熵；T表熱量傳輸時介質之絕對溫度。式(2.21)中，等號右邊之第一項與熱傳導作用有關，第二項與熱之強制對流作用有關，第三項與介質內部之熱源有關。茲引用式(2.13)之關係式，則式(2.21)可表為：

$$\dot{S}^* = -\left[\frac{q_i - n\rho_f c_{vf}\theta\left(\dot{v}_i - \dot{u}_i\right)}{T}\right]_{,i} - \frac{\left[q_i - n\rho_f c_{vf}\theta\left(\dot{v}_i - \dot{u}_i\right)\right]\theta_{,i}}{T^2} + \frac{W}{T} \text{ ，} \tag{2.22}$$

式中等號右邊之第一項係多孔介質與環境因熱量傳輸所引致之熵，其餘兩項則為介質內部因熱量變化所引致之熵。由熱力學第二定律知，式(2.22)中等號右邊之第二項需滿足 Claussius-Duhem 不等式，即

$$-\frac{\left[q_i - n\rho_f c_{vf}\theta\left(\dot{v}_i - \dot{u}_i\right)\right]\theta_{,i}}{T^2} \geq 0 \text{。} \tag{2.23}$$

基於此，由式(2.22)知，Claussius-Duhem 不等式(2.23)亦可表為：

$$\frac{dS^*}{dt} + \left[\frac{q_i - n\rho_f c_{vf}\theta\left(\dot{v}_i - \dot{u}_i\right)}{T}\right]_{,i} - \frac{W}{T} \geq 0 \text{ 。} \tag{2.24}$$

由式(2.20)與式(2.21)知：

$$\dot{U}^* = \sigma_{ij}\dot{\varepsilon}_{ij} + \sigma \dot{\in} + T\dot{S}^* \text{。} \tag{2.25}$$

茲引用 Helmholtz 自由能（free energy）F^*作研析，令

$$F^* = U^* - TS^*，\tag{2.26}$$

上式對時間 t 微分一次，並引用式(2.25)之關係式，則可推導出：

$$\begin{aligned}\dot{F}^* &= \dot{U}^* - \dot{T}S^* - T\dot{S}^* \\ &= \sigma_{ij}\dot{\varepsilon}_{ij} + \sigma\dot{\in} + T\dot{S}^* - \dot{T}S^* - T\dot{S}^* \\ &= \sigma_{ij}\dot{\varepsilon}_{ij} + \sigma\dot{\in} - \dot{T}S^*。\end{aligned}\tag{2.27}$$

式(2.26)中之 F^* 係以 ε_{ij} 、$\in$ 與 T 為基本變數，即 $F^* = F^*\left(\varepsilon_{ij}, \in, T\right)$，其對時間 t 之微分可表為：

$$\dot{F}^* = \frac{\partial F^*}{\partial \varepsilon_{ij}}\dot{\varepsilon}_{ij} + \frac{\partial F^*}{\partial \in}\dot{\in} + \frac{\partial F^*}{\partial T}\dot{T}\ ，\tag{2.28}$$

比較式(2.27)與式(2.28)，可研討出以下之關係式：

$$\sigma_{ij} = \frac{\partial F^*}{\partial \varepsilon_{ij}}\ ，\tag{2.29a}$$

$$\sigma = \frac{\partial F^*}{\partial \in}\ ，\tag{2.29b}$$

$$S^* = -\frac{\partial F^*}{\partial T}。\tag{2.29c}$$

上式為建立多孔介質熱彈性力學之組成律（constitutive law）的基礎。

2-2 多孔介質熱彈性力學之組成律

茲考慮介質於初始狀態下 $\left(T = T_0\right)$ 時，$\varepsilon_{ij} = 0$ 且 $\in = 0$，以此為參考狀態，對 F^* 作 Taylor 級數展開，可得：

$$F^*\left(\varepsilon_{ij},\in,T\right)=F^*\left(0,0,T_0\right)+\frac{\partial F^*\left(0,0,T_0\right)}{\partial\varepsilon_{ij}}\varepsilon_{ij}+\frac{\partial F^*\left(0,0,T_0\right)}{\partial\in}\in+\frac{\partial F^*\left(0,0,T_0\right)}{\partial T}\left(T-T_0\right)$$

$$+\frac{1}{2}\left[\frac{\partial^2F^*\left(0,0,T_0\right)}{\partial\varepsilon_{ij}\partial\varepsilon_{kl}}\varepsilon_{ij}\varepsilon_{kl}+\frac{\partial^2F^*\left(0,0,T_0\right)}{\partial\in^2}\in^2+\frac{\partial^2F^*\left(0,0,T_0\right)}{\partial T^2}\left(T-T_0\right)^2\right.$$

$$+2\frac{\partial^2F^*\left(0,0,T_0\right)}{\partial\varepsilon_{ij}\partial\in}\varepsilon_{ij}\in+2\frac{\partial^2F^*\left(0,0,T_0\right)}{\partial\varepsilon_{ij}\partial T}\varepsilon_{ij}\left(T-T_0\right)$$

$$\left.+2\frac{\partial^2F^*\left(0,0,T_0\right)}{\partial\in\partial T}\in\left(T-T_0\right)\right]+\cdots\text{，}\tag{2.30}$$

其中$F^*\left(0,0,T_0\right)$係介質於初始狀態下之自由能。若考慮介質於初始狀態下之應變為零，則其初始應力為零，亦無熵之變化，即$\sigma_{ij}\left(0,0,T_0\right)=0$、$\sigma\left(0,0,T_0\right)=0$且$S^*\left(0,0,T_0\right)=0$。基於此，由式(2.29a)至式(2.29c)知：

$$\frac{\partial F^*\left(0,0,T_0\right)}{\partial\varepsilon_{ij}}=\sigma_{ij}\left(0,0,T_0\right)=0\text{，}\tag{2.31a}$$

$$\frac{\partial F^*\left(0,0,T_0\right)}{\partial\in}=\sigma\left(0,0,T_0\right)=0\text{，}\tag{2.31b}$$

$$\frac{\partial F^*\left(0,0,T_0\right)}{\partial T}=-S^*\left(0,0,T_0\right)=0\text{，}\tag{2.31c}$$

將式(2.31a)至式(2.31c)代入式(2.30)，並考慮初始狀態下之 Helmholtz 自由能為零，即$F^*\left(0,0,T_0\right)=0$，則式$\left(2.30\right)$可改寫為：

$$F^*\left(\varepsilon_{ij},\in,T\right)=\frac{1}{2}\left[\frac{\partial^2F^*\left(0,0,T_0\right)}{\partial\varepsilon_{ij}\partial\varepsilon_{kl}}\varepsilon_{ij}\varepsilon_{kl}+\frac{\partial^2F^*\left(0,0,T_0\right)}{\partial\in^2}\in^2+\frac{\partial^2F^*\left(0,0,T_0\right)}{\partial T^2}\left(T-T_0\right)^2\right.$$

$$+2\frac{\partial^2F^*\left(0,0,T_0\right)}{\partial\varepsilon_{ij}\partial\in}\varepsilon_{ij}\in+2\frac{\partial^2F^*\left(0,0,T_0\right)}{\partial\varepsilon_{ij}\partial T}\varepsilon_{ij}\left(T-T_0\right)$$

$$\left.+2\frac{\partial^2F^*\left(0,0,T_0\right)}{\partial\in\partial T}\in\left(T-T_0\right)\right]+\cdots\text{。}\tag{2.32}$$

式(2.30)代入式(2.29a)與式(2.29b)中，並引用式(2.31a)、式(2.31b)與$F^*\left(0,0,T_0\right)=0$之關係式，則可推導出：

$$\sigma_{ij}\left(\varepsilon_{ij},\in,T\right)=\frac{\partial^2 F^*\left(0,0,T_0\right)}{\partial\varepsilon_{ij}\partial\varepsilon_{kl}}\varepsilon_{kl}+\frac{\partial^2 F^*\left(0,0,T_0\right)}{\partial\varepsilon_{ij}\partial\in}\in+\frac{\partial^2 F^*\left(0,0,T_0\right)}{\partial\varepsilon_{ij}\partial T}\left(T-T_0\right)，\quad (2.33a)$$

$$\sigma\left(\varepsilon_{ij},\in,T\right)=\frac{\partial^2 F^*\left(0,0,T_0\right)}{\partial\varepsilon_{ij}\partial\in}\varepsilon_{ij}+\frac{\partial^2 F^*\left(0,0,T_0\right)}{\partial\in^2}\in+\frac{\partial^2 F^*\left(0,0,T_0\right)}{\partial\in\partial T}\left(T-T_0\right)。\quad (2.33b)$$

上式忽略了高階微分項次，此為合理之考慮，符合$\left|\theta/T_0\right|<<1$之基本假設。

茲定義式(2.32)中之相關係數如以下所示：

$$\frac{\partial^2 F^*\left(0,0,T_0\right)}{\partial\varepsilon_{ij}\partial\varepsilon_{kl}}=C_{ijkl}\ ，\quad (2.34a)$$

$$\frac{\partial^2 F^*\left(0,0,T_0\right)}{\partial\varepsilon_{ij}\partial\in}=\alpha_{ij}\ ，\quad (2.34b)$$

$$\frac{\partial^2 F^*\left(0,0,T_0\right)}{\partial\varepsilon_{ij}\partial T}=-\beta_{ij}，\quad (2.34c)$$

$$\frac{\partial^2 F^*\left(0,0,T_0\right)}{\partial\in\partial T}=-\gamma\ ，\quad (2.34d)$$

$$\frac{\partial^2 F^*\left(0,0,T_0\right)}{\partial T^2}=m，\quad (2.34e)$$

$$\frac{\partial^2 F^*\left(0,0,T_0\right)}{\partial\in^2}=R\ ，\quad (2.34f)$$

則式(2.32)、式(2.33a)與式(2.33b)可分別表為：

$$F^*\left(\varepsilon_{ij},\in,T\right)=\frac{1}{2}C_{ijkl}\varepsilon_{ij}\varepsilon_{kl}+\frac{1}{2}R\in^2+\frac{1}{2}m\theta^2+\alpha_{ij}\varepsilon_{ij}\in-\beta_{ij}\varepsilon_{ij}\theta-\gamma\varepsilon\theta\ ，\quad (2.35)$$

$$\sigma_{ij}\left(\varepsilon_{ij},\in,T\right)=C_{ijkl}\varepsilon_{kl}+\alpha_{ij}\in-\beta_{ij}\theta，\quad (2.36a)$$

$$\sigma\left(\varepsilon_{ij},\in,T\right)=\alpha_{ij}\varepsilon_{ij}+R\in-\gamma\theta\ 。\quad (2.36b)$$

若引用式(2.36a)與式(2.36b)之關係式，對相關變數作適當之微分運算，可知：

$$\left[\frac{\partial \sigma_{ij}}{\partial \varepsilon_{kl}}\right]_{\in,T} = C_{ijkl}\ ,\tag{2.37a}$$

$$\left[\frac{\partial \sigma_{ij}}{\partial \in}\right]_{\varepsilon,T} = \left[\frac{\partial \sigma}{\partial \varepsilon_{ij}}\right]_{\in,T} = \alpha_{ij}\ ,\tag{2.37b}$$

$$\left[\frac{\partial \sigma_{ij}}{\partial T}\right]_{\varepsilon,\in} = -\beta_{ij}\ ,\tag{2.37c}$$

$$\left[\frac{\partial \sigma}{\partial \in}\right]_{\varepsilon,T} = R\ ,\tag{2.37d}$$

$$\left[\frac{\partial \sigma}{\partial T}\right]_{\varepsilon,\in} = -\gamma\ ,\tag{2.37e}$$

式中多孔介質之熱力學常數C_{ijkl}、α_{ij}與R係於等溫度狀況下測得，β_{ij}與γ係於等應變狀況下測得，其中C_{ijkl}為與固體介質有關之力學常數，α_{ij}係與固體介質及孔隙流體同時相關之耦合力學常數，R是與孔隙流體有關之力學常數，β_{ij}和γ則為與介質溫度有關之力學常數。若考慮多孔介質之力學性質為等向性，則式(2.35)可表為：

$$F^*\left(\varepsilon_{ij},\in,T\right) = N\varepsilon_{ij}\varepsilon_{ij} + \frac{1}{2}A\varepsilon^2 + \frac{1}{2}R\in^2 + Q\varepsilon\in + \frac{1}{2}m\theta^2 - \gamma_t\varepsilon\theta - \overline{\gamma}_t\in\theta\ ,\tag{2.38}$$

其中係數A、N為與固體介質有關之力學常數，係數Q係與固體介質及孔隙流體同時相關之耦合力學常數，係數m為與溫度變化有關之力學常數，其物理意義將於式(2.47)至式(2.59)中加以研討。γ_t及$\overline{\gamma}_t$之物理意義將於式(2.42)至式(2.45)中予以說明。基於此，式(2.36a)與式(2.36b)可改寫為：

$$\sigma_{ij} = 2N\varepsilon_{ij} + \left(A\varepsilon + Q\in -\gamma_t\theta\right)\delta_{ij}\ ,\tag{2.39a}$$

$$\sigma = R\in + Q\varepsilon - \overline{\gamma}_t\theta\ 。\tag{2.39b}$$

令式(2.39a)中之下標$i = j$，則

$$\sigma_{kk} = \left(3A + 2N\right)\varepsilon + 3Q\in -3\gamma_t\theta\ 。\tag{2.40}$$

式(2.39a)與式(2.39b)作適當之反轉換，可得：

$$\varepsilon_{ij}=\frac{1}{2N}\sigma_{ij}-\frac{1}{3A+2N}\left[\frac{A}{2N}\sigma_{kk}+Q\in-\gamma_t\theta\right]\delta_{ij}\ ,\tag{2.41a}$$

$$\in=\frac{\sigma}{R}-\frac{Q}{R}\varepsilon+\frac{\overline{\gamma}_t}{R}\theta\ 。\tag{2.41b}$$

為研討係數γ_t與$\overline{\gamma}_t$之物理意義，茲考慮多孔介質不受外力作用，並可自由膨脹，則多孔介質受熱作用時，內部無應力變化。基於此，令式(2.41a)中之下標$i=j$，則式(2.41a)與式(2.41b)可改寫為：

$$\varepsilon^{\circ}=-\frac{3Q}{3A+2N}\in^{\circ}+\frac{3\gamma_t}{3A+2N}\theta\ ,\tag{2.42a}$$

$$\in^{\circ}=-\frac{Q}{R}\varepsilon^{\circ}+\frac{\overline{\gamma}_t}{R}\theta\ ,\tag{2.42b}$$

式中$\varepsilon^{\circ}=u^{\circ}_{k,k}$，$\in^{\circ}=v^{\circ}_{k,k}$，$\varepsilon^{\circ}$與$\in^{\circ}$分別表固體介質與孔隙流體因溫度升高$\theta$時，體積之自由膨脹量。解析式(2.42a)與式(2.42b)，可推導出ε°與$\in^{\circ}$如以下所示：

$$\varepsilon^{\circ}=\frac{3R\gamma_t-3Q\overline{\gamma}_t}{\left(3A+2N\right)R-3Q^2}\theta\ ,\tag{2.43a}$$

$$\in^{\circ}=\frac{\left(3A+2N\right)\overline{\gamma}_t-3Q\gamma_t}{\left(3A+2N\right)R-3Q^2}\theta\ 。\tag{2.43b}$$

由物理試驗得知，固體介質與孔隙流體受熱時之體積膨脹量分別與溫度變化量成正比[43]，因此，若令α_s與α_f分別為固體介質與孔隙流體之線性熱膨脹係數（linear thermal expansion coefficient），則

$$\varepsilon^{\circ}=3\alpha_s\theta\ ,\tag{2.44a}$$

$$\in^{\circ}=3\alpha_f\theta\ 。\tag{2.44b}$$

比較式(2.43a)、式(2.43b)與式(2.44a)、式(2.44b)，令對應之係數相同，可解析得γ_t與$\overline{\gamma}_t$如以下所示：

$$\gamma_t=\left(3A+2N\right)\alpha_s+3Q\alpha_f\ ,\tag{2.45a}$$

$$\overline{\gamma}_t = 3\left(Q\alpha_s + R\alpha_f\right)\ ,\tag{2.45b}$$

上式清楚研討出係數γ_t與$\overline{\gamma}_t$之物理意義。其中γ_t與$\overline{\gamma}_t$同時受固體介質及孔隙流體之相關力學常數的影響，而γ_t及$\overline{\gamma}_t$會隨α_s及α_f之增加而增加。同時，由式(2.39a)、式(2.39b)、式(2.41a)與式(2.41a)知：

$$\left[\frac{\partial\sigma_{ij}}{\partial T}\right]_{\varepsilon,\in} = -\gamma_t\delta_{ij}\ ,\tag{2.46a}$$

$$\left[\frac{\partial\sigma}{\partial T}\right]_{\varepsilon,\in} = -\overline{\gamma}_t\ ,\tag{2.46b}$$

$$\left[\frac{\partial\varepsilon}{\partial\sigma_{kk}}\right]_{T,\in} = \frac{1}{3A+2N}\ ,\tag{2.46c}$$

$$\left[\frac{\partial\varepsilon}{\partial T}\right]_{\in,\sigma_{kk}} = 3\alpha_s + \frac{9Q}{3A+2N}\alpha_f\ ,\tag{2.46d}$$

$$\left[\frac{\partial\varepsilon}{\partial\in}\right]_{T,\sigma_{kk}} = -\frac{3Q}{3A+2N}\ ,\tag{2.46e}$$

$$\left[\frac{\partial\varepsilon}{\partial\sigma}\right]_{T,\varepsilon} = \frac{1}{R}\ ,\tag{2.46f}$$

$$\left[\frac{\partial\in}{\partial T}\right]_{\varepsilon,\sigma} = 3\frac{Q}{R}\alpha_s + 3\alpha_f\ ,\tag{2.46g}$$

$$\left[\frac{\partial\in}{\partial\varepsilon}\right]_{T,\sigma} = -\frac{Q}{R}\ 。\tag{2.46h}$$

由於考慮微小應變理論適用，因此式(2.38)中，與ε_{ij}有關之高次項可以忽略。若將與溫度有關之高次項以函數$G(\theta)$表示，則式(2.38)可改寫為：

$$F^*\left(\varepsilon_{ij},\in,T\right) = N\varepsilon_{ij}\varepsilon_{ij} + \frac{1}{2}A\varepsilon^2 + \frac{1}{2}R\in^2 + Q\varepsilon\in -\gamma_t\varepsilon\theta - \overline{\gamma}_t\in\theta + G(\theta)\ ,\tag{2.47}$$

將上式代回式(2.29c)，可得：

$$S^* = \gamma_t \varepsilon + \overline{\gamma}_t \in -\frac{\partial G}{\partial T} \text{ ，} \tag{2.48}$$

式中S^*係以ε_{ij}、$\in$與T為變數之函數，因此，S^*之全微分可表為：

$$dS^* = \left[\frac{\partial S^*}{\partial \varepsilon_{ij}}\right]_{\in,T} d\varepsilon_{ij} + \left[\frac{\partial S^*}{\partial \in}\right]_{\varepsilon,T} d \in + \left[\frac{\partial S^*}{\partial T}\right]_{\varepsilon,\in} dT \text{ ，} \tag{2.49}$$

式中$T\left[\partial S^* / \partial T\right]_{\varepsilon,\in}$表單位多孔介質體積內每升高一度$C$所需要的熱量，令：

$$c_v = T\left[\frac{\partial S^*}{\partial T}\right]_{\varepsilon,\in} \text{ ，} \tag{2.50}$$

其中c_v稱為固定應變下多孔介質之比熱，且：

$$c_v = (1-n)\rho_s c_{vs} + n\rho_f c_{vf} \text{ ，} \tag{2.51}$$

其中係數c_{vs}與c_{vf}分別表單位質量之固體介質與孔隙流體每升高一度C所需要之熱量；ρ_s與ρ_f分別為固體介質與孔隙流體之密度。

由式(2.48)知：

$$dS^* = \gamma_t d\varepsilon + \overline{\gamma}_t d \in -\frac{\partial^2 G}{\partial T^2} dT \text{ ，} \tag{2.52}$$

比較式(2.49)與式(2.52)知：

$$c_v = -T\frac{\partial^2 G}{\partial T^2} \text{ ，} \tag{2.53}$$

上式對變數T作適當之積分，可推導出：

$$\frac{\partial G}{\partial T} = -\int_{T_0}^{T} \frac{c_v}{T} dT = -c_v \ln \frac{T}{T_0} \text{ ，} \tag{2.54a}$$

$$G(\theta)=-\int_{T_0}^{T}\left[\int_{T_0}^{T}\frac{c_v}{T}dT\right]dT \text{ 。} \tag{2.54b}$$

因此，式(2.48)可表為：

$$S^*=\gamma_t\varepsilon+\overline{\gamma}_t\in+c_v\ln\frac{T}{T_0} \text{ 。} \tag{2.55}$$

因為考慮$|\theta/T_0|<<1$，故

$$\ln\frac{T}{T_0}=\ln\left(1+\frac{\theta}{T_0}\right)=\frac{\theta}{T_0}-\frac{1}{2}\left(\frac{\theta}{T_0}\right)^2+\frac{1}{3}\left(\frac{\theta}{T_0}\right)^3-+\cdots\cong\frac{\theta}{T_0} \text{ 。} \tag{2.56}$$

基於此，式(2.55)可表為：

$$S^*\cong\gamma_t\varepsilon+\overline{\gamma}_t\in+\frac{c_v}{T_0}\theta \text{ ，} \tag{2.57}$$

式中等號右邊之第一項與第二項係考慮溫度與固體介質及孔隙流體因交互作用所引致之熵的變化，而最後一項則考慮介質因熱傳導作用所引致之熵。茲引用式(2.56)之關係式，並對變數T作適當之積分，可將式(2.54b)改寫為：

$$G(\theta)=-\frac{c_v}{2T_0}\theta^2 \text{ 。} \tag{2.58}$$

將$G(\theta)$代回式(2.47)，推導出：

$$F^*\left(\varepsilon_{ij},\in,T\right)=N\varepsilon_{ij}\varepsilon_{ij}+\frac{1}{2}A\varepsilon^2+\frac{1}{2}R\in^2+Q\varepsilon\in-\gamma_t\varepsilon\theta-\overline{\gamma}_t\in\theta-c_v\frac{\theta^2}{2T_0} \text{ 。} \tag{2.59}$$

比較式(2.38)與式(2.59)知，係數$m=-c_v/T_0$。式(2.59)中等號右邊之前四項與固體介質及孔隙流體之應變量有關，而最後一項僅與溫度變化有關，其餘項次則是考慮固體介質、孔隙流體及介質溫度變化量間之交互作用效應。

2-3 熱傳導方程式

由式(2.21)知，熵平衡方程式可表為：

$$\frac{dS^*}{dt} = -\frac{1}{T}\left[q_{i,i} - n\rho_f c_{vf}\theta_{,i}\left(\dot{v}_i - \dot{u}_i\right) - W \right]。 \tag{2.60}$$

又由式(2.23)知，若考慮介質之熱傳導性質為等向性，則熱傳導方程式可表示如下：

$$q_i = -\lambda_t \theta_{,i} + n\rho_f c_{vf}\theta\left(\dot{v}_i - \dot{u}_i\right)， \tag{2.61}$$

其中λ_t為多孔介質之熱傳導係數。

式(2.61)代回式(2.60)，並引用式(2.13)之關係式，可推導出：

$$T\frac{dS^*}{dt} = \lambda_t \theta_{,kk} + W 。 \tag{2.62}$$

又由式(2.55)知：

$$T\dot{S}^* = \left(\gamma_t \dot{\varepsilon} + \overline{\gamma}_t \dot{\in}\right)T + c_v \dot{T}， \tag{2.63}$$

式(2.62)與式(2.63)作適當之化簡，可推導出：

$$\lambda_t \theta_{,kk} + W = \left(\gamma_t \dot{\varepsilon} + \overline{\gamma}_t \dot{\in}\right)T + c_v \dot{T} ， \tag{2.64a}$$

或

$$\theta_{,kk} - \frac{c_v}{\lambda_t}\dot{\theta} - \frac{\gamma_t}{\lambda_t}T\dot{u}_{k,k} - \frac{\overline{\gamma}_t}{\lambda_t}T\dot{\in} + \frac{W}{\lambda_t} = 0 。 \tag{2.64b}$$

由於過高或過低之溫度變化會使孔隙流體由液體轉變成氣體或固態，本研究暫不考慮此種情況，因此介質之溫度變化量θ符合$\left|\theta/T_0\right| << 1$之基本假設，故式(2.64b)之非線性方程式可據以改寫為線性偏微分方程式如以下所示：

$$\theta_{,kk}-\frac{c_v}{\lambda_t}\dot{\theta}-\frac{\gamma_t T_0}{\lambda_t}\dot{u}_{k,k}-\frac{\overline{\gamma}_t T_0}{\lambda_t}\dot{\in}+\frac{W}{\lambda_t}=0\ ,\tag{2.65}$$

上式係以多孔介質之位移u_i、孔隙流體之體積變化量$\in$及介質溫度變化量θ為主要變數，為物理問題之第一個基本方程式。

茲引用式(2.9)與式(2.39b)之關係式，將熱傳導方程式(2.65)改寫為以介質位移u_i、超額孔隙流體壓力p及介質溫度變化量θ為主要變數，如以下所示：

$$\theta_{,kk}-\frac{1}{\lambda_t}\left(c_v+\overline{\gamma}_t^{\,2}\frac{T_0}{R}\right)\dot{\theta}-\frac{T_0}{\lambda_t}\left(\gamma_t-\frac{Q}{R}\overline{\gamma}_t\right)\dot{u}_{k,k}+\frac{\overline{\gamma}_t T_0}{\lambda_t}\frac{n}{R}\dot{p}+\frac{W}{\lambda_t}=0\ 。\tag{2.66}$$

若進一步考慮飽和多孔介質有變形但無體積變化，即將多孔介質模擬為不可壓縮，則：

$$(1-n)\varepsilon+n\in=0\ ,\tag{2.67}$$

上式與式(2.39b)作比較，可知：

$$Q,R\to\infty\ ,\ \frac{Q}{R}=\frac{1-n}{n}\ 。\tag{2.68}$$

上式代入式(2.66)，並引用式(2.45a)與式(2.45b)，可進一步將熱傳導方程式改寫為：

$$\theta_{,kk}-\frac{c_v}{\lambda_t}\dot{\theta}-\frac{(2G+3\lambda)\alpha_s T_0}{\lambda_t}\dot{u}_{k,k}+\frac{3\left[(1-n)\alpha_s+n\alpha_f\right]T_0}{\lambda_t}\dot{p}+\frac{W}{\lambda_t}=0\ ,\tag{2.69}$$

其中多孔介質之力學常數$2G+3\lambda=3A+2N-3Q^2/R$[3]，G與λ分別為多孔介質之剪力係數與*Lame*常數。其餘四個基本方程式將於以下兩節所說明之連續方程式及力平衡方程式推導出。

2-4 連續方程式

本節擬研討多孔介質熱彈性力學之連續方程式。有關孔隙流體在孔隙中之流動應遵循 Darcy 定律：

$$\sigma_{,i} = b\left(\dot{v}_i - \dot{u}_i\right)，\tag{2.70}$$

式中 Darcy 係數 $b = n^2 \gamma_f / k$，n 為多孔介質之孔隙率，γ_f 係孔隙流體之單位體積重量，k 為多孔介質之滲透係數（permeability）。

茲引用式(2.39b)，將 Darcy 定律式(2.70)改寫為：

$$Q\varepsilon_{,i} + R\in_{,i} - \overline{\gamma}_t\theta_{,i} - b\left(v_i - u_i\right) = 0，\tag{2.71}$$

上式取其散度（divergence），並利用 $\varepsilon = u_{i,i}$ 之關係式，可推導出：

$$Qu_{i,ikk} + R\in_{,kk} - \overline{\gamma}_t\theta_{,kk} - b\left(\dot{\in} - \dot{u}_{k,k}\right) = 0，\tag{2.72}$$

上式係以多孔介質之位移 u_i、孔隙流體之體積變化量 $\in$ 及介質溫度變化量 θ 為主要變數。

由於考慮流體之體積變化量較不易測得，而超額孔隙流體壓力較易量測，因此，引用式(2.9)與式(2.39b)之關係式，消去其中之 $\in$ 與 σ，推導出以多孔介質位移 u_i、超額孔隙流體壓力 p 與介質溫度變化量 θ 為主要變數之連續方程式如以下所示：

$$-\frac{k}{\gamma_f}p_{,kk} + \frac{n^2}{R}\dot{p} + n\frac{Q+R}{R}\dot{u}_{k,k} - 3n\left(\frac{Q}{R}\alpha_s + \alpha_f\right)\dot{\theta} = 0。\tag{2.73}$$

若考慮飽和多孔介質不可壓縮，即引用式(2.68)之關係式，則連續方程式(2.73)可進一步加以化簡：

$$-\frac{k}{\gamma_f}p_{,kk} + \dot{u}_{k,k} - 3\left[\left(1-n\right)\alpha_s + n\alpha_f\right]\dot{\theta} = 0。\tag{2.74}$$

2-5 力平衡方程式

本節研討多孔介質之力平衡方程式。由牛頓第二定律知，作用於多孔介質上之總應力 τ_{ij} 需滿足力平衡原理 $\tau_{ij,j}=0$。基於此，若不考慮徹體力及慣性力的影響，並引用 Terzaghi[1]的有效應力觀念，則式(2.8)中之總應力需滿足力平衡方程式，即：

$$\sigma_{ij,j}+\sigma_{,i}=0\text{。} \tag{2.75}$$

將式(2.39a)與式(2.39b)之組成律方程式代入上式，可得：

$$2N\varepsilon_{ij,j}+\left(A+Q\right)\varepsilon_{,i}+\left(Q+R\right)\in_{,i}-\left(\gamma_t+\overline{\gamma}_t\right)\theta_{,i}=0\text{，} \tag{2.76}$$

上式引用 $\varepsilon_{ij}=\left(u_{i,j}+u_{j,i}\right)\big/2$ 與 $\varepsilon=\varepsilon_{kk}=u_{k,k}$ 之關係式，則可推導出以多孔介質位移 u_i、孔隙流體體積應變 $\in$ 與介質溫度變化量 θ 為主要變數之力平衡方程式：

$$Nu_{i,kk}+\left(A+N+Q\right)u_{k,ki}+\left(Q+R\right)\in_{,i}-\left(\gamma_t+\overline{\gamma}_t\right)\theta_{,i}=0\text{，} \tag{2.77}$$

上式中之下標 $i=1,2,3$，故式(2.77)包含三個基本方程式。上式與式(2.65)及式(2.72)組成等向性多孔介質熱彈性力學之五個基本方程式。

若考慮以超額孔隙流體壓力 p 取代孔隙流體體積變化量 $\in$ 為基本變數，則可引用式(2.6)與式(2.39b)之關係式，將力平衡方程式改寫為：

$$Nu_{i,kk}+\left(A+N-\frac{Q^2}{R}\right)u_{k,ki}-n\frac{Q+R}{R}p_{,i}-\left(\gamma_t-\frac{Q}{R}\overline{\gamma}_t\right)\theta_{,i}=0\text{，} \tag{2.78}$$

式中 Biot[3]所引用之力學常數與常見之力學常數的關係如以下所示：

$$N=G\text{，}A+N-\frac{Q^2}{R}=\left(2\eta-1\right)G\text{，}\eta=\frac{1-\nu}{1-2\nu}\text{，} \tag{2.79}$$

其中 G 為多孔介質之剪力係數，ν 為多孔介質於排水情況下所測得之柏松比。茲考慮多孔介質於受熱應力過程中有形狀改變，但無體積的變化，即將多孔介質視為不可壓縮，如式(2.67)所示。基於此，引用式(2.45a)、式(2.45b)、式(2.68)及式(2.79)之關係式，則力平衡方程式(2.78)可進一步改寫為常見之形式：

$$Gu_{i,kk}+(2\eta-1)Gu_{k,ki}-p_{,i}-(2G+3\lambda)\alpha_s\theta_{,i}=0\text{。} \tag{2.80}$$

上式中之下標$i=1,2,3$，故式(2.80)包含三個基本方程式。式(2.69)、式(2.74)及式(2.80)組成耦合三維熱壓密理論之五個基本控制方程式。

2-6 熱壓密模式的整理

由以上說明知，所建立之三維熱壓密模式係以土壤位移u_i、孔隙流體壓力p及介質溫度變化量θ為主要變數。數學模擬中，將飽和土壤模擬為均質且等向性之彈性體，若考慮孔隙流體與固體土粒均不可壓縮，則所建立的耦合三維熱壓密理論之基本方程式如式(2.69)、式(2.74)及式(2.80)所示，整理如下：

$$Gu_{i,kk}+(2\eta-1)Gu_{k,ki}-p_{,i}-(2G+3\lambda)\alpha_s\theta_{,i}=0\text{，} \tag{2.81a}$$

$$-\frac{k}{\gamma_f}p_{,kk}+\dot{u}_{k,k}-3\left[(1-n)\alpha_s+n\alpha_f\right]\dot{\theta}=0\text{，} \tag{2.81b}$$

$$\theta_{,kk}-\frac{c_v}{\lambda_t}\dot{\theta}-\frac{(2G+3\lambda)\alpha_s T_0}{\lambda_t}\dot{u}_{k,k}+\frac{3\left[(1-n)\alpha_s+n\alpha_f\right]T_0}{\lambda_t}\dot{p}+\frac{W}{\lambda_t}=0\text{，} \tag{2.81c}$$

式中W表作用於多孔介質內部之熱源。若考慮熱傳導方程式(2.81c)僅與介質溫度變化量θ有關，而式(2.81a)與式(2.81b)仍保持相同，則所建立之熱壓密模式係考慮為部分耦合情況，如 Booker 等人[12-14]所建立之熱壓密方程式：

$$Gu_{i,kk}+(2\eta-1)Gu_{k,ki}-p_{,i}-(2G+3\lambda)\alpha_s\theta_{,i}=0\text{，} \tag{2.82a}$$

$$-\frac{k}{\gamma_t}p_{,kk}+\dot{u}_{k,k}-3\left[(1-n)\alpha_s+n\alpha_f\right]\dot{\theta}=0\text{，} \tag{2.82b}$$

$$\theta_{,kk}-\frac{c_v}{\lambda_t}\dot{\theta}+\frac{W}{\lambda_t}=0\text{。} \tag{2.82c}$$

有關非耦合之熱壓密模式係進一步考慮連續方程式僅與孔隙流體壓力有關。基於此，三維熱壓密模式之控制方程式可表為：

$$Gu_{i,kk}+(2\eta-1)Gu_{k,ki}-p_{,i}-(2G+3\lambda)\alpha_s\theta_{,i}=0\text{，} \tag{2.83a}$$

$p_{,kk}=0$ ， (2.83b)

$$\theta_{,kk}-\frac{c_v}{\lambda_t}\dot{\theta}+\frac{W}{\lambda_t}=0 \text{ 。} \tag{2.83c}$$

本研究基於所研討出之耦合、部分耦合與非耦合三維熱壓密模式，解析淺層暨深層熱源影響之飽和土壤力學行為變化，並加以研討、比較。就大地工程適用範圍而言，耦合三維熱壓密模式可應用於飽和地層情況，而部分耦合及非耦合三維熱壓密模式則可應用於水分較少之情況，其相關之研究請參見第三章之說明。

2-7 所引用的土壤參數之量測方法

有關各參數之量測方法，簡述如下：

α_s 由式(2.44a)知$\varepsilon^{o}=3\alpha_s\theta$，亦即量測固體介質因溫度升高所引致之體積自由膨脹量，便可得到固體介質之線性熱膨脹係數。

α_f 由式(2.44b)知$\in^{o}=3\alpha_f\theta$，亦即量測孔隙流體因溫度升高所引致之體積自由膨脹量，便可得到孔隙流體之線性熱膨脹係數。

c_s 於隔熱裝置中，量測每公斤之固體介質因溫度升高一度所需之熱量，即可得固體介質之比熱。

c_f 於隔熱裝置中，量測每公斤之孔隙流體因溫度升高一度所需之熱量，即可得孔隙流體之比熱。

λ_t 由 *Fourier* 定律知$q_i=-\lambda_t\theta_{,i}$。因此，於隔熱裝置中，控制柱狀土壤試體兩端之溫度，當其達成熱平衡時，其溫度梯度$\theta_{,i}$可由土樣兩端之溫度變化及試體長度求得，而單位時間內通過單位面積之熱量q_i亦可測出，因此熱傳導係數便可推導出。

G 由共振柱試驗法可得土壤之剪力係數。

ν 由共振柱試驗法亦可得楊氏係數，並配合上述之剪力係數，再利用$G=E/[2(1+\nu)]$之關係式，即可推導出柏松比。

ρ_s 由基本土壤力學之物性試驗，即可得固體介質密度。

ρ_f 量測孔隙流體單位體積之質量，即可得知孔隙流體之密度。

k 由定水頭、變水頭或壓密試驗測定法，可測到土壤之滲透係數。

n 由基本土壤力學之物性試驗，即可測得土壤之孔隙率。

2-8 參考文獻

1. Terzaghi, K., *Theoretical Soil Mechanics*, John Wiley & Sons, New York, N.Y., pp. 256-296 (1943).

2. Biot, M.A., "General Theory of Three-Dimensional Consolidation," *J. Appl. Phys.*, Vol. 12, No. 2, pp. 155-164 (1941).

3. Biot, M.A., "Theory of Elasticity and Consolidation for a Porous Anisotropic Solid," *J. Appl. Phys.*, Vol. 26, No. 2, pp. 182-185 (1955).

4. Bear, J. and M.Y. Corapcioglu, "Mathematical Model for Regional Land Subsidence Due to Pumping, 1, Integrated Aquifer Subsidence Equations Based on Vertical Displacement Only," *Water Resour. Res.*, Vol. 17, No. 7, pp. 937-946 (1981).

5. Verruijt, A., "Elastic Storage of Aquifers," *Flow Through Porous Media*, Academic Press, R.J.M. de Wiest (ed.), New York, pp. 331-376 (1969).

6. Rice, J.R. and M.P. Cleary, "Some Basic Stress Diffusion Solutions for Fluid-Saturated Elastic Porous Media with Compressible Constituents," *Rev. Geophys. Space Phys.*, Vol. 14, No. 2, pp. 227-241 (1976).

7. Schiffman, R.L., "A Thermoelastic Theory of Consolidation," *Environmental and Geophysical Heat Transfer*, *ASME*, C.J. Cremers et. al. (eds.), Vol. 4, New York, N.Y., pp.78-84 (1971).

8. Bear, J. and M.Y Corapcioglu, "A Mathematical Model for Consolidation in a Thermoelastic Aquifer Due to Hot Water Injection or Pumping," *Water Resour. Res.*, Vol. 17, No. 3, pp.723-736 (1981).

9. Aboustit, B.L., S.H. Advani, and J.K. Lee, "Variational Principles and Finite Element Simulations for Thermo-Elastic Consolidation," *Int. J. Numer. Anal. Methods Geomech.*, Vol. 9, No. 1, pp.46-69 (1985).

10. Geraminegad, M. and S.K. Saxena, "A Coupled Thermoelastic Model for Saturated-Unsaturated Porous Media," *Geotechnique*, Vol. 36, No. 4, pp. 539-550 (1986).

11. McTigue, D.F., "Flow to a Heated Borehole in Porous, Thermoelastic Rock: Analysis," *Water Resour. Res.*, Vol. 26, No. 8, pp. 1763-1774 (1990).

12. Booker, J.R. and C. Savvidou, "Consolidation Around a Point Heat Source," *Int. J. Numer. Anal. Methods Geomech.*, Vol. 9, pp. 173-184 (1985).

13. Booker, J.R. and C. Savvidou, "Consolidation Around a Spherical Heat Source," *Int. J. Solids Structures*, Vol. 20, No. 11/12, pp. 1079-1090 (1984).

14. Booker, J.R. and C. Savvidou, "Consolidation Around a Heat Source Buried Deep in a Porous Thermoelastic Medium with Anisotropic Flow Properties," *Int. J. Numer. Anal. Methods Geomech.*, Vol. 13, No. 1, pp. 75-90 (1989).

15. 國科會/原能會，「國科會/原能會科技學術合作研究計畫」，

http://www.aec.gov.tw/www/ policy/plans/files/nsc-aec-95-1.pdf (2006)。

16. Bear, J. and M.Y. Corapcioglu, "Mathematical Model for Consolidation in a Thermoelastic Aquifer Due to Hot Water Injection or Pumping," *Water Resour. Res.*, Vol. 17, No. 3, pp. 723-736 (1981).

17. Mei, C.C. and P.A. Tyvand, "Thermal Consolidation of Thick and Soft Soil Layer," *J. Engng. Mech.*, ASCE, Vol. 114, No. 6, pp. 990-1010 (1988).

18. Sarger, F.J., "Around Freezing in Construction," *Soil Mechanics and Foundations Division*, Vol. 94, No. SM1, pp. 131-158 (1968).

19. Brownell, D.H., Jr., S.K. Garg, and J.W. Pritchett, "Governing Equations for Geothermal Reservoirs," *Water Resour. Res.*, Vol. 13, No. 6, pp. 929-934 (1977).

20. Geraminegad, M. and S.K. Saxena, "Coupled Thermoelastic Model for Saturated-Unsaturated Porous Media," *Geotechnique*, Vol. 36, No. 4, pp. 539-550 (1986).

21. Houston, S.L., W.N. Houston, and N.D. Williams, "Thermo-Mechanical Behavior of Seafloor Sediments," *J. Geotech. Engng.*, Vol. 111, No. 11, pp. 1249-1263 (1985).

22. Ma, C. and T. Hueckel, "Stress and Pore Pressure in Saturated Clay Subjected to Heat from Radioactive Waste: A Numerical Simulation," *Can. Geotech. J.*, Vol. 29, pp. 1087-1094 (1992).

23. Lu, John C.-C. and Feng-Tsai Lin, "The Transient Ground Surface Displacements Due to a Point Sink/Heat Source in an Elastic Half-Space," *Geotechnical Special Publication, No. 148, ASCE,* pp. 210-218 (2006).

24. Lu, John C.-C. and Feng-Tsai Lin, "Thermo-consolidation Due to a Point Heat Source Buried in a Poroelastic Half Space," *Proceedings of the 3rd IASTED International Conference on Environmental Modelling and Simulation*, Honolulu, Hawaii, U.S.A., pp. 48-53 (2007).

25. Lu, John C.-C. and Feng-Tsai Lin, "Transient Solutions for a Cross-anisotropic Stratum Subjected to a Deep Point Heat Source," *Proceedings of ASME Applied Mechanics and Materials Conference*, Austin, Texas, U.S.A., Abstract in CD (2007).

26. Lu, John C.-C., "Long-Term Behaviors of a Buried Deep Point Heat Source in a Transversely Isotropic Thermoelastic Porous Medium," *Chung Hua Journal of Science and Engineering*, Vol. 4, No. 1, pp. 11-22 (2006).

27. Edgar, T.V., J.D. Nelson, and D.B. McWhorter, "Nonisothermal Consolidation in Unsaturated Soil," *J. Geotech. Engng.*, Vol. 115, No. 10, pp. 1351-1372 (1989).

28. Britto, A.M., C. Savvidou, D.V. Maddocks, M.J. Gunn, and J.R. Booker, "Numerical and Centrifuge Modelling of Coupled Heat Flow and Consolidation Around Hot Cylinders Buried in Clay," *Geotechnique*, Vol. 39, No. 1, pp. 13-25 (1989).

29. Seneviratne, H.N., J.P. Carter, and J.R. Booker, "Analysis of Fully Coupled Thermomechanical Behaviour Around a Rigid Cylindrical Heat Source Buried in Clay," *Int. J. Numer. Anal. Methods Geomech.*, Vol. 18, pp. 177-203 (1994).

30. Wang, X., E. Pan, and A.K. Roy, "Three-dimensional Green's Functions for a Steady Point Heat Source in a Functionally Graded Half-space and Some Related Problems," *Int. J. Engng. Science*, Vol. 45, No. 11, pp. 939-950 (2007).

31. Simoes, N. and A. Tadeu, "Fundamental Solutions for Transient Heat Transfer by Conduction and Convection in an Unbounded, Half-space, Slab and Layered Media in the Frequency Domain," *Engng. Analysis with Boundary Elements*, Vol. 29, No. 12, pp. 1130-1142 (2005).

32. Tadeu, A. and N. Simoes, "Three-dimensional Fundamental Solutions for Transient Heat Transfer by Conduction in an Unbounded Medium, Half-space, Slab and Layered Media," *Engng. Analysis with Boundary Elements*, Vol. 30, No. 5, pp. 338-349 (2006).

33. Shendeleva, M.L., "Instantaneous Line Heat Source Near a Plane Interface," *J. Appl. Phys.*, Vol. 95, No. 5, pp. 2839-2845 (2004).

34. Mishuris, G. and M. Wrobel, "Coupled FEM-BEM Approach for Axisymetrical Heat Transfer Problems," *Diffusion and Defect Data. Pt A Defect and Diffusion Forum*, *Duffusion in Solid and Liquids III*, Vol. 273-276, pp. 740-745 (2008).

35. Bai, B., "Thermal Consolidation of Layered Porous Half-space to Variable Thermal Loading," *Applied Mathematics and Mechanics (English ed.)*, Vol. 27, No. 11, pp. 1531-1539 (2006).

36. Sheng, J.C., J. Liu, W.C. Zhu, D. Elsworth, and J.X. Liu, "Stress Analysis of a Borehole in Saturated Rocks under in Situ Mechanical, Hydrological and Thermal Interactions," *Energy Sources, Part A: Recovery, Utilization and Environmental Effects*, Vol. 30, No. 2, pp. 157-169 (2008).

37. Li, N., B. Chen, F. Chen, and X. Xu, 2006, "Coupled Heat-Moisture-Mechanic Model of the Frozen Soil," *Cold Regions Science and Technology*, Vol. 31, No. 3, pp. 199-205 (2006).

38. Bai, B. and J. He, "Thermal Consolidation of Saturated Porous Media under Cyclic Temperature Loading," *Geotechnical Special Publication*, No. 148, *Advances in Unsaturated Soil, Seepage, and Environmental Geotechnics - Proceedings of the GeoShanghai Conference*, pp. 240-245 (2006).

39. Bai, B., "Response of Saturated Porous Media Subjected to Local Thermal Loading on the Surface of Semi-infinite Space," *Acta Mechanica Sinica/Lixue Xuebao*, Vol. 22, No. 1, pp. 54-61 (2006).

40. Murad, M.A. and J.H. Cushman, "Thermomechanical Theories for Swelling Porous Media with Microstructure," *Int. J. Engng. Science*, Vol. 38, No. 5, pp. 517-564 (2000).

41. Cui, Y.-J. and W.-M. Ye, "Modeling of Thermo-mechanical Volume Change Behavior of Saturated Clays," *Yanshilixue Yu Gongcheng Xuebao/Chinese*

Journal of Rock Mechanics and Engineering, Vol. 24, No. 21, pp. 3903-3910 (2005).

42. Nowacki, W., *Thermoelasticity*, Pergamon Press, New York, 556 p (1986).

43. Benson, H., *Unversity Physics*, John Wiley & Sons, Inc., New York, pp. 363-366 (1991).

2-9 符號說明

A, N, Q, R	Biot 所定義之多孔介質力學常數
b	Darcy 係數，$b = n^2 \gamma_f / k$
c_v	固定應變下飽和土壤之比熱
c_{vs}, c_{vf}	固定應變下土粒與孔隙流體之比熱
E	多孔介質之楊氏係數
F^*	Helmholtz 自由能，$F^* = U^* - TS^*$
G	多孔介質之剪力係數
h	熱點源之埋置深度
$\vec{h}$	通過單位多孔介質面積之熱流率向量
k	多孔介質之滲透係數
$\dot{K}$	儲存於多孔介質內之動能的增率
$\dot{L}$	外力作用於多孔介質所引致之功率
n	土壤之孔隙率
p	超額孔隙水壓力
q	單位時間單位多孔介質體積內所產生之熱量
q_i	單位時間內通過單位多孔介質面積之熱量
Q	單位時間內多孔介質內部所產生之熱量
$\dot{Q}$	單位時間內多孔介質內部之熱量增率
S^*	單位多孔介質體積內因熱量變化所引致之熵
t	時間變數
T	多孔介質受熱影響後之溫度
T_i	作用於多孔介質之總表面應力
T_0	多孔介質之初始溫度
T_i^s, T_i^f	作用於固體介質與孔隙流體之表面應力
u_i	圓柱座標系統下多孔介質之位移分量

u_i^{o}　　彈性介質之位移分量

$\dot{U}$　　儲存於多孔介質內之內能的增率

U^*　　單位多孔介質體積內所儲存之內能

v_i　　孔隙流體之位移分量

W　　單位時間單位多孔介質體積內所產生之熱量

x_i^s, x_i^f　　固體介質與孔隙流體之徵體力

希臘字母

α_s, α_f　　固體土粒與孔隙流體之線性熱膨脹係數

α_u　　參數，$\alpha_u = (1-n)\alpha_s + n\alpha_f$

γ_f　　孔隙流體之單位體積重量

$\gamma_t, \overline{\gamma}_t$　　式(2.45a)與(2.45b)所定義之參數

$\delta(x)$　　Dirac-delta 函數

δ_{ij}　　Kronecker delta

$\varepsilon, \in$　　多孔介質與孔隙流體之體積應變量，$\varepsilon = u_{i,i}$，$\in = v_{i,i}$

$\varepsilon_{ij}, \in_{ij}$　　多孔介質與孔隙流體之應變量

ε^{o}　　彈性介質之體積應變量

η　　參數，$\eta = (1-\nu)/(1-2\nu)$

θ　　多孔介質之溫度變化量，$\theta = T - T_0$

λ　　多孔介質之 Lame 常數

λ_t　　多孔介質之熱傳導係數

ν　　多孔介質之柏松比

ρ　　多孔介質之密度，$\rho = (1-n)\rho_s + n\rho_f$

ρ_s, ρ_f　　固體土粒與孔隙流體之密度

σ 作用於孔隙流體面積上之應力

σ_{ij} 作用於固體土粒面積上之有效應力

τ_{ij} 作用於飽和土壤之總應力

第三章　研究內容

3-1　前言

本計畫基於第二章所研討出之基本方程式，擬進一步分別研討出以下所述三種問題之閉合解，包括：瞬時熱源與穩定熱源所引致等向性地層之溫度分佈、深層點熱源所引致橫向等向性地層之熱彈性行為的解析、瞬時點熱源所引致半無限域地層之熱彈性行為的解析，其解析過程與其解析結果分別詳述於第 3-2 節、第 3-3 節與第 3-4 節中。

根據第 3-2 節之研究結果得知：(1)在「穩定熱源」作用的考量下，隨著熱源作用時間的增加，地層中各點之溫度會逐漸上升，最後形成一穩態平衡。(2)在「瞬時熱源」作用的考量下，隨著熱源作用時間的增加，地層中各點之溫度會先上升然後逐漸下降，最後上升之地層溫度會完全消失。

根據第 3-3 節之解析結果得知：(1)地層中所有的熱彈性行為均與觀察點至熱源的距離有關，且與地層之線性熱膨脹係數成正比，但與地層之熱傳導係數成反比；另外，由研究結果得知，地層之溫度變化及位移變化均與地層剪力模數無關。(2)地層之橫向等向性特徵對地層之熱應力有明顯的影響，例如當線性熱膨脹係數比 α_{sr}/α_{sz} 增加時，所引致之熱應力會明顯上升；但線性熱傳導係數比 $\lambda_{tr}/\lambda_{tz}$ 增加時，所引致之熱應力會明顯下降。(3)在等向性地層的考慮下，徑向正向熱應力 σ_{rr} 與垂直正向熱應力 σ_{zz} 之比值介於 0.5~2.0，而環向正向熱應力 $\sigma_{\theta\theta}$ 與垂直正向熱應力 σ_{zz} 之比值則介於 0.5~1.0。

根據第 3-4 節之研討結果得知：(1)引用熱彈性力學與多孔介質彈力理論之類比關係，瞬時熱源所引致之地層熱彈性行為可轉換為瞬時抽水問題的解。(2)瞬時熱源作用於地層時，地層之各項熱彈性反應會在一瞬間達到極大值，然後再逐漸消散，因將地層模擬為彈性介質，故各種地層之熱彈性行為變化最後都會完全消失。(3)地表因瞬時熱源作用所引致之最大水平位移約為最大垂直位移的 38.5%，顯然瞬時熱源作用時，所引起的地表水平位移是不宜忽略的。

本文所研討出之閉合解，可應用於檢驗數值模擬之分析程序是否正確無誤，亦可作為探討其他熱源類型所引致相關問題之研究基礎。

3-2 瞬時熱源與穩定熱源所引致等向性地層之溫度分佈

摘 要

本文旨在探討等向性之半無限域地層因瞬時熱源與穩定熱源所引致的地層溫度增量的分佈，所建立之數學模式，係考慮半無限域地層之熱流性質為等向性，並考慮地表邊界為恆溫情況。本文是引用 Laplace 與 Hankel 積分轉換方法解析所建立之數學模式，所研討出之理論解為與時間有關之暫態閉合解。

關鍵詞：瞬時熱源，穩定熱源，半無限域，閉合解

Abstract

The study of this paper is focus on the distributions of temperature increments of the stratum due to instantaneous and steady heat sources in the isotropic stratum of a half space. In the mathematical model, the thermal properties of the stratum are regarded as isotropic. Besides, the half space ground surface is considered as isothermal. Using Laplace and Hankel integral transform techniques on the formulated mathematical model. Theoretical transient closed-form solutions are obtained in this study.

Keywords: Instantaneous heat source, Steady heat source, Half space, Closed-form solution

一、前言

引起地層溫度發生變化的因素有很多，例如氣候變化、冰凍工法、溫泉開發及垃圾掩埋場的悶燒現象等均會造成地層溫度的改變，尤其台灣位於歐亞大陸板塊和菲律賓板塊交界處，火山地形與斷層多，地層中之熱量潛能也較高，且岩層中有岩漿在流動等，進行深層開挖時，均會導致地層溫度的改變，而影響地層的力學行為等。近年來，核廢料掩埋問題亦廣受重視，由於核廢料為放射性物質，如埋置不當，將對生態環境造成傷害。目前的處理方式之一是擬將核廢料埋置於深層岩層中，為了避免高溫之核廢料破壞岩層之穩定性，導致生物圈之破壞，因此，探討熱源作用於地層所引致之地層力學行為變化，至為重要。

本文旨在探討等向性（isotropic）地層受「瞬時熱源」與「穩定熱源」影響時之溫度分佈場，所引用之理論為熱彈性力學理論。Booker 等人[1-4]曾探討地層之熱壓密問題的解析解，開始對點熱源、球體熱源、分層地層受衰減熱源影響、以及異向性滲流情況之熱壓密問題等加以探討。Giraud 與 Rousset[5]曾探討球狀熱源對多孔彈性介質之影響，Claesson 和 Probert[6]等學者則解析矩形熱源對半無限域多孔介質地層之影響，Lu 與 Lin[7，8]、Lu[9]、Lin 與 Lu[10]均曾研討過掩埋熱源對地層位移與溫度變化等的影響。相關之研究，不勝枚舉。本文擬將地層模擬為一半無限域，並引用熱彈性力學理論，將地層的熱流與力學等性質模擬為等向性，理論模式中會引用力平衡、能量守恆與 Fourier 熱傳導定律等。

若熱源的形狀大小相對於其影響範圍較小，則可將熱源形狀模擬為一個點，本文即採用點熱源模擬熱作用源。本文所考慮之熱作用源的類型包括兩類，一類是熱源之作用強度持續不變，稱為「穩定熱源」；另一類是熱源的熱量僅在極短時間釋放出來，此類

熱源稱為「瞬時熱源」。本文擬分別探討這兩類熱源所引致的地層溫度分佈的閉合解（Closed-form Solution）。解析數學模式時，會採用 Hankel 和 Laplace 積分轉換方法，分別對空間變數 r 與時間變數 t 作積分轉換，推導出地層受點熱源影響時之溫度分佈場的閉合解。點熱源作用問題之解尚有其他應用，例如可將點熱源作用問題的解作熱源形狀之線積分、面積分或體積分等，推導出其他形狀熱源作用問題的解；另外，許多數值模擬程序是否正確無誤，亦可引用本文所研討出之閉合解進行檢驗。為了解不同型態熱源對地層溫度分佈的影響，本文將針對所研討出之閉合解進行參數影響分析，繪製各樣的圖形並加以比較，用以說明等向性地層受點熱源影響時之溫度分佈場的變化。

二、數學模式

如圖 1 所示，若採用圓柱座標系統 (r,θ,z)，並讓座標 z 軸通過點熱源，則本文所建立之軸對稱非耦合熱彈性力學數學模式中的基本方程式，如以下所示[7]：

$$G\nabla^2 u_r + \frac{G}{1-2\nu}\frac{\partial \varepsilon}{\partial r} - G\frac{u_r}{r^2} - \beta\frac{\partial \vartheta}{\partial r} = 0 \ , \tag{1a}$$

$$G\nabla^2 u_z + \frac{G}{1-2\nu}\frac{\partial \varepsilon}{\partial z} - \beta\frac{\partial \vartheta}{\partial z} = 0 \ , \tag{1b}$$

$$\lambda_t \nabla^2 \vartheta - c_\varepsilon \frac{\partial \vartheta}{\partial t} + q(r,z,t) = 0 \ , \tag{1c}$$

其中 G 、ν 與 λ_t 分別為地層之剪力模數（Shear Modulus）、柏松比（Poisson's Ratio）與熱傳導係數（Thermal Conductivity）；參數 $c_\varepsilon = \rho c$，ρ 與 c 分別為地層之質量密度（Mass Density）與比熱（Specific Heat）；參數 $\beta = (2G+3\lambda)\alpha_s$，$\lambda$ 與 α_s 分別為地層之 Lame 常數與線性熱膨脹係數（Linear Thermal Expansion Coefficient）；地層之體積應變量 $\varepsilon = \partial u_r/\partial r + u_r/r + \partial u_z/\partial z$ ，式中 u_r 與 u_z 則是地層在水平方向與垂直方向之位移變化量；符號 ϑ 是地層溫度增量；微分運算子 $\nabla^2 = \partial^2/\partial r^2 + 1/r\,\partial/\partial r + \partial^2/\partial z^2$ ；$q(r,z,t)$ 則與熱源變率有關，本文擬分別探討「穩定熱源」及「瞬時熱源」所引致的地層溫度分佈，並考慮點熱源之掩埋深度為 h 。

若考慮「穩定熱源」，則 $q(r,z,t)$ 可表為：

$$q(r,z,t) = \frac{Q_c}{2\pi r}\delta(r)\delta(z-h)u(t) \ , \tag{2a}$$

若考慮「瞬時熱源」，則 $q(r,z,t)$ 可表為：

$$q(r,z,t) = \frac{Q_0}{2\pi r}\delta(r)\delta(z-h)\delta(t) \ , \tag{2b}$$

其中 Q_c 表單位時間內所釋出的熱量；Q_0 則表極短時間內所釋出的熱量；$\delta(x)$ 為 Dirac-delta 函數；$u(t)$ 係單位階梯函數（Unit Step Function）。

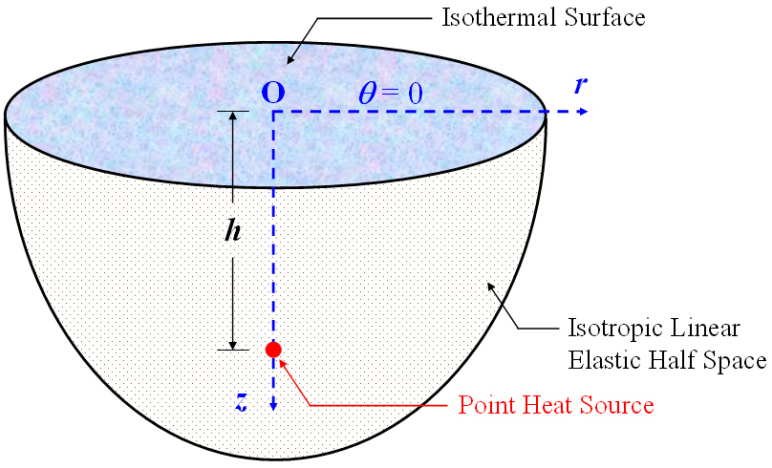

圖 1　半無限域中之單點熱源示意圖

本文所考慮之初始條件（Initial Condition）為：一開始的時候（$t \to 0^+$），所有的位移變量暨地層溫度增量均為零。亦即：

$$\lim_{t\to 0^+}\left\{u_r(r,z,t),u_z(r,z,t),\vartheta(r,z,t)\right\}=\{0,0,0\}\ 。 \tag{3}$$

所需考慮之邊界條件包括 $z=0$ 之地表邊界條件及 $z\to\infty$ 之無限深遠處的邊界條件。本文是考慮地表邊界無熱應力 τ_{ij} 之變化且為恆溫情況，而無限深遠處之地層位移與地層溫度增量則考慮為不受單點熱源的影響。基於此，地表邊界條件可表為：

$$\tau_{zz}(r,0,t)=\frac{2G\nu}{1-2\nu}\left[\frac{\partial u_r(r,0,t)}{\partial r}+\frac{u_r(r,0,t)}{r}\right]+\frac{2G(1-\nu)}{1-2\nu}\frac{\partial u_z(r,0,t)}{\partial z}=0\ ， \tag{4a}$$

$$\tau_{rz}(r,0,t)=G\left[\frac{\partial u_r(r,0,t)}{\partial z}+\frac{\partial u_z(r,0,t)}{\partial r}\right]=0\ ， \tag{4b}$$

$$\vartheta(r,0,t)=0\ 。 \tag{4c}$$

而無限深遠處之邊界條件則可表為：

$$\lim_{z\to\infty}\left\{u_r(r,z,t),u_z(r,z,t),\vartheta(r,z,t)\right\}=\{0,0,0\}\ 。 \tag{5}$$

式(1)~(5)組成問題之數學模式。本文將專注於單點熱源所引致的地層溫度增量分佈之解析，係引用 Hankel 與 Laplace 積分轉換方法解析出地層的溫度增量分佈。

三、地層溫度增量之解析

因所研討的主要對象為地層之溫度增量分佈，故所需探討的主要基本方程式為式(1c)。茲引用 Hankel 積分轉換對式(1c)中之空間座標變數 r 作零階之積分轉換，再對其中之時間變數 t 作 Laplace 積分轉換，並引用式(3)與溫度增量有關之初始條件，則式(1c)可改寫為：

$$\lambda_t\left(\frac{d^2}{dz^2}-\xi^2\right)\tilde{\vartheta}(z;\xi,s)-c_\varepsilon s\tilde{\vartheta}(z;\xi,s)+\tilde{q}(z;\xi,s)=0 \ ， \tag{6}$$

若考慮「穩定熱源」，則 $\tilde{q}(z;\xi,s)$ 可表為：

$$\tilde{q}(z;\xi,s)=\frac{Q_c}{2\pi s}\delta(z-h) \ ， \tag{7a}$$

若考慮「瞬時熱源」，則 $\tilde{q}(z;\xi,s)$ 可表為：

$$\tilde{q}(z;\xi,s)=\frac{Q_0}{2\pi}\delta(z-h) \ ， \tag{7b}$$

其中 ξ 與 s 分別為 Hankel 積分轉換參數與 Laplace 積分轉換參數；符號 $\tilde{\vartheta}(z;\xi,s)$ 與 $\tilde{q}(z;\xi,s)$ 分別定義如下：

$$\tilde{\vartheta}(z;\xi,s)=\int_0^\infty rL\{\vartheta(r,z,t)\}J_0(\xi r)\,dr \ ， \tag{8a}$$

$$\tilde{q}(z;\xi,s)=\int_0^\infty rL\{q(r,z,t)\}J_0(\xi r)\,dr \ ， \tag{8b}$$

式中 $J_0(\xi r)$ 表零階之第一種類型的 Bessel 函數；$L\{\vartheta(r,z,t)\}$ 與 $L\{q(r,z,t)\}$ 表地層溫度增量 $\vartheta(r,z,t)$ 與熱源變率 $q(r,z,t)$ 之 Laplace 積分轉換，亦即：

$$L\{\vartheta(r,z,t)\}=\int_0^\infty \vartheta(r,z,t)exp(-st)\,dt \ ， \tag{9a}$$

$$L\{q(r,z,t)\}=\int_0^\infty q(r,z,t)exp(-st)\,dt \ 。 \tag{9b}$$

若考慮「穩定熱源」，則式(6)之通解（General Solution）為：

$$\tilde{\vartheta}(z;\xi,s)=2\eta G\frac{1}{\xi}\frac{s}{c}C_1exp\left(\sqrt{\xi^2+\frac{s}{c}}\,z\right)+2\eta G\frac{1}{\xi}\frac{s}{c}C_2exp\left(-\sqrt{\xi^2+\frac{s}{c}}\,z\right)$$

$$+\frac{Q_c}{4\pi\lambda_t}\frac{1}{s}\frac{1}{\sqrt{\xi^2+\frac{s}{c}}}exp\left(-\sqrt{\xi^2+\frac{s}{c}}\left|z-h\right|\right)\ , \tag{10a}$$

若考慮「瞬時熱源」，則式(6)之通解為：

$$\tilde{\vartheta}\left(z;\xi,s\right)=2\eta G\frac{1}{\xi}\frac{s}{c}C_1 exp\left(\sqrt{\xi^2+\frac{s}{c}}\,z\right)+2\eta G\frac{1}{\xi}\frac{s}{c}C_2 exp\left(-\sqrt{\xi^2+\frac{s}{c}}\,z\right)$$

$$+\frac{Q_0}{4\pi\lambda_t}\frac{1}{\sqrt{\xi^2+\frac{s}{c}}}exp\left(-\sqrt{\xi^2+\frac{s}{c}}\left|z-h\right|\right)\ , \tag{10b}$$

其中$c=\lambda_t/c_\varepsilon$；式(10a)-(10b)中之符號$C_1$與$C_2$係與參數$\xi$和$s$有關，其解析需藉由積分轉換域之邊界條件方可求出。式(4c)與式(5)中與地層溫度增量ϑ有關之邊界條件作Laplace與Hankel積分轉換後可得：

$$\tilde{\vartheta}\left(0;\xi,s\right)=0\ , \tag{11a}$$

$$\tilde{\vartheta}\left(\infty;\xi,s\right)=0\ 。 \tag{11b}$$

引用式(11a)與(11b)即可解析出式(10a)與(10b)中之符號C_1與C_2。經仔細研討與計算後，並引用適當之數學使用手冊[11]，滿足積分轉換域邊界條件之地層溫度增量如以下所示。

若考慮「穩定熱源」，則積分轉換域$\left(z;\xi,s\right)$之地層溫度增量為：

$$\tilde{\vartheta}\left(z;\xi,s\right)=\frac{Q_c}{4\pi\lambda_t}\frac{1}{s}\frac{1}{\sqrt{\xi^2+\frac{s}{c}}}\left[exp\left(-\sqrt{\xi^2+\frac{s}{c}}\left|z-h\right|\right)-exp\left(-\sqrt{\xi^2+\frac{s}{c}}\left(z+h\right)\right)\right]\ , \tag{12a}$$

若考慮「瞬時熱源」，則積分轉換域$\left(z;\xi,s\right)$之地層溫度增量為：

$$\tilde{\vartheta}\left(z;\xi,s\right)=\frac{Q_0}{4\pi\lambda_t}\frac{1}{\sqrt{\xi^2+\frac{s}{c}}}\left[exp\left(-\sqrt{\xi^2+\frac{s}{c}}\left|z-h\right|\right)-exp\left(-\sqrt{\xi^2+\frac{s}{c}}\left(z+h\right)\right)\right]\ 。 \tag{12b}$$

式(12a)-(12b)表單點熱源所引致積分轉換域$\left(z;\xi,s\right)$的地層溫度增量分佈，$\tilde{\vartheta}\left(z;\xi,s\right)$尚需進行Laplace積分反轉換與Hankel積分反轉換，方能推導出實數域$\left(r,z,t\right)$之地層溫度增量$\vartheta\left(r,z,t\right)$。$\tilde{\vartheta}\left(z;\xi,s\right)$之Laplace與Hankel積分反轉換的定義為：

$$\vartheta\left(r,z,t\right)=\frac{1}{2\pi i}\int_{\alpha-i\infty}^{\alpha+i\infty}\int_0^\infty \xi\tilde{\vartheta}\left(z;\xi,s\right)J_0\left(\xi r\right)e^{st}d\xi ds\ 。 \tag{13}$$

式(12a)與式(12b)引用式(13)所示之 Laplace 與 Hankel 積分反轉換，即可研討出問題之解。經審慎研討後，獲得以下所示之閉合解。

若考慮「穩定熱源」，則實數域的地層溫度增量 $\vartheta(r,z,t)$ 之閉合解為：

$$\vartheta(r,z,t)=\frac{Q_c}{4\pi\lambda_t}\left\{\frac{1}{\sqrt{r^2+(z-h)^2}}erfc\left[\frac{\sqrt{r^2+(z-h)^2}}{2\sqrt{ct}}\right]-\frac{1}{\sqrt{r^2+(z+h)^2}}erfc\left[\frac{\sqrt{r^2+(z+h)^2}}{2\sqrt{ct}}\right]\right\}, \tag{14a}$$

若考慮「瞬時熱源」，則實數域的地層溫度增量 $\vartheta(r,z,t)$ 之閉合解為：

$$\vartheta(r,z,t)=\frac{Q_0}{8\pi\lambda_t}\frac{1}{\sqrt{\pi ct^3}}\left\{exp\left[-\frac{r^2+(z-h)^2}{4ct}\right]-exp\left[-\frac{r^2+(z+h)^2}{4ct}\right]\right\}, \tag{14b}$$

其中 $erfc(x)$ 為補誤差函數（Complementary Error Function）。在 $t\to\infty$ 之長期地層溫度增量的考慮下，式(14a)與式(14b)可進一步加以改寫，如以下所示。

若考慮「穩定熱源」，則 $t\to\infty$ 之長期地層溫度增量 $\vartheta(r,z,t)$ 的閉合解為：

$$\vartheta(r,z,\infty)=\frac{Q_c}{4\pi\lambda_t}\left[\frac{1}{\sqrt{r^2+(z-h)^2}}-\frac{1}{\sqrt{r^2+(z+h)^2}}\right], \tag{15a}$$

若考慮「瞬時熱源」，則 $t\to\infty$ 之長期地層溫度增量 $\vartheta(r,z,t)$ 的閉合解為：

$$\vartheta(r,z,\infty)=0\ 。 \tag{15b}$$

式(15a)的工程意義是，在「穩定熱源」的作用下，長期而言地層會形成一穩定的溫度增量分佈。而式(15b)的工程意義是，「瞬時熱源」所引致的地層溫度增量會逐漸消失，當 $t\to\infty$ 時，地層的溫度增量已完全消失。以上本文所研討出之閉合解，可應用於檢驗數值模擬之分析程序是否正確無誤，亦可作為探討其他熱源類型所引致相關問題的研究基礎。

四、數值結果

為瞭解所研討出之單點熱源所引致的地層溫度增量，圖 2 是根據式(14a)所繪製之單點「穩定熱源」所引致的無因次化地層溫度增量分佈。圖 2 分別考慮無因次化時間因子 $\sqrt{ct/h^2}=1$、2、3、∞時之地層溫度增量分佈，由圖 2 得知，在熱源持續作用的考量下，隨著熱源作用延時的增加，地層中各點之溫度會逐漸上升，最後形成一穩態平衡，如圖 2(d)所示。

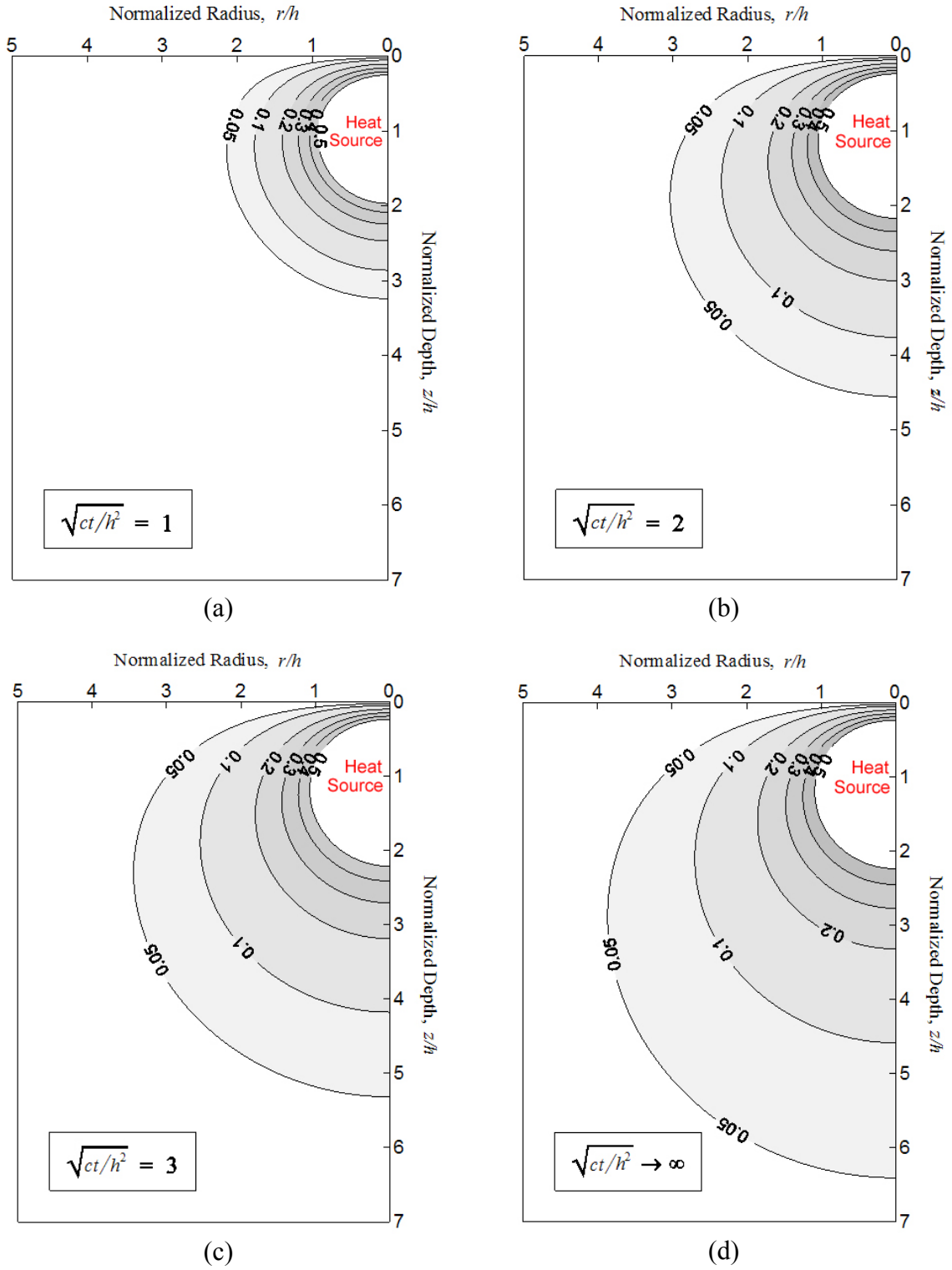

圖 2　單點「穩定熱源」所引致之無因次化地層溫度增量 $\vartheta(r,z,t)/[Q_c/4\pi\lambda_t h]$

圖 3 則是根據式(14b)所繪製之單點「瞬時熱源」所引致的無因次化地層溫度增量分佈，分別考慮無因次化時間因子 $\sqrt{ct/h^2}$ =0.4、0.6、0.8、1.0 時之地層溫度增量分佈。由圖 3 得知，在「瞬時熱源」的考量下，隨著時間的增加，地層中各點之溫度會先上升然後逐漸下降，最後地層溫度增量會完全消失。

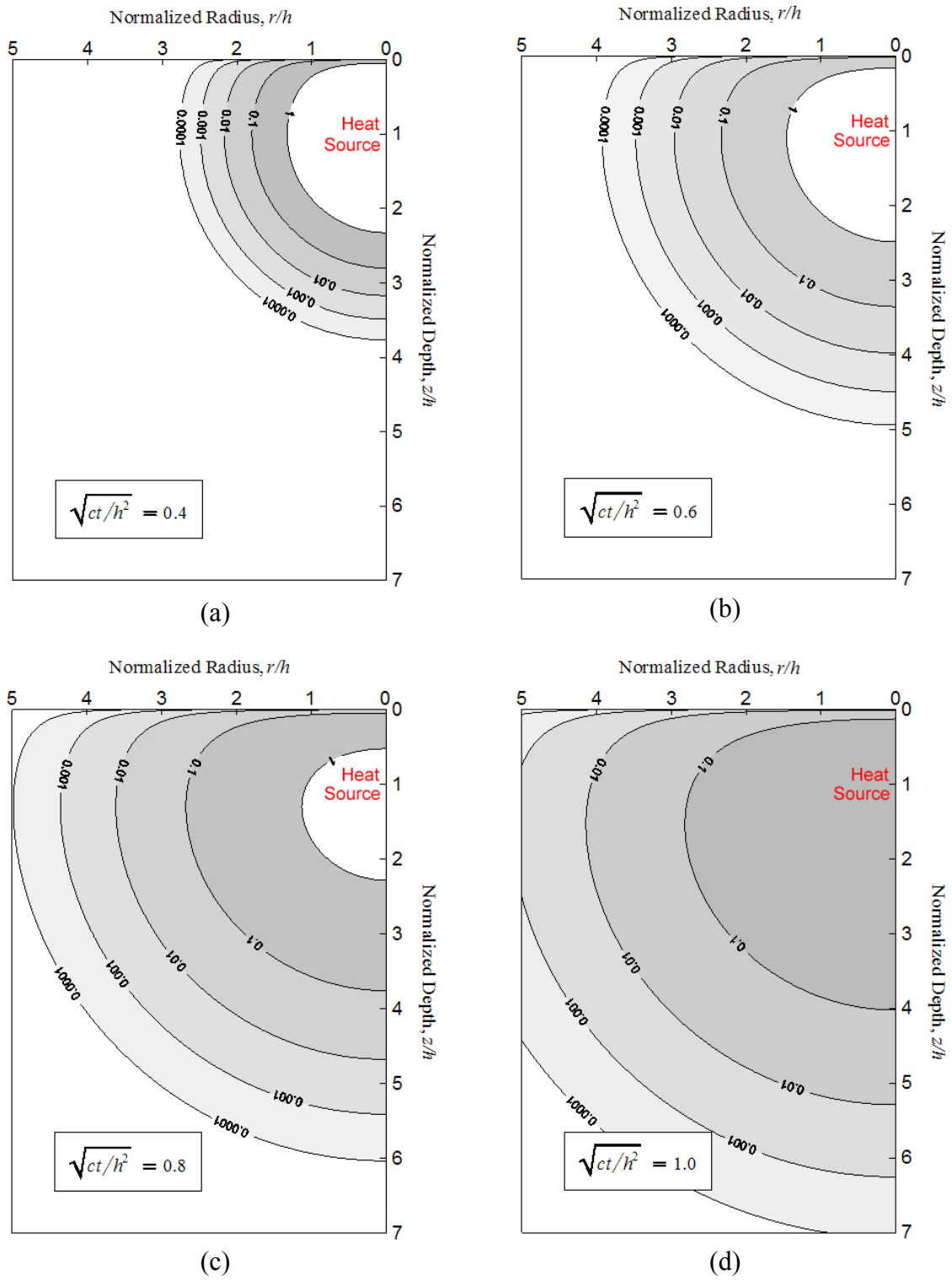

圖 3　單點「瞬時熱源」所引致之無因次化地層溫度增量 $\vartheta(r,z,t)/\left[cQ_0/8\pi^{1.5}\lambda_t h^3\right]$

五、結論

本文係將地層模擬為均質等向性的半無限域地層，分別考慮「穩定熱源」及「瞬時熱源」這兩種熱作用源所引起的地層溫度增量分佈，是以 Laplace 與 Hankel 積分轉換方法推導出問題的閉合解。根據本文之研究得知以下結論：

1. 在「穩定熱源」作用的考量下，隨著熱源作用時間的增加，地層中各點之溫度會逐漸上升，最後形成一穩態平衡。
2. 在「瞬時熱源」作用的考量下，隨著熱源作用時間的增加，地層中各點之溫度會先上升然後逐漸下降，最後上升之地層溫度會完全消失。
3. 本文所研討出之閉合解，可應用於檢驗數值模擬之分析程序是否正確無誤，亦可作為探討其他熱源類型所引致相關問題之研究基礎。

六、誌謝

本文在國科會計畫 NSC-98-2815-C-216-007-E 暨中華大學計畫 CHU-98-2815-C-216-007-E 之經費援助下，始得以順利完成，特此申謝。

七、參考文獻

1. Booker, J.R. and Savvidou, C., "Consolidation Around a Spherical Heat Source," *Int. J. Solids Structures*, Vol. 20, pp. 1079-1090, 1984.
2. Booker, J.R. and Savvidou, C., "Consolidation Around a Point Heat Source," *Int. J. Numer. Anal. Methods Geomech.*, Vol. 9, pp. 173-184, 1985.
3. Small, J.C. and Booker, J.R., "The Behaviour of Layered Soil or Rock Containing a Decaying Heat Source," *Int. J. Numer. Anal. Methods Geomech.*, Vol. 10, pp. 501-519, 1986.
4. Savvidou, C. and Booker, J.R., "Consolidation Around a Heat Source Buried Deep in a Porous Thermoelastic Medium with Anisotropic Flow Properties," *Int. J. Numer. Anal. Methods Geomech.*, Vol. 13, pp. 75-90, 1989.
5. Giraud, A. and Rousset, G., "Consolidation Around a Volumic Spherical Decaying Heat Source," *J. Thermal Stresses*, Vol. 18, pp. 513-536, 1995.
6. Claesson, J. and Probert, T., "Thermoelastic Stress Due to a Rectangular Heat Source in a Semi-infinite Medium. Presentation of an Analytical Solution," *Engineering Geology*, Vol. 49, pp. 223-229, 1998.
7. Lu, J. C.-C., and Lin, F.-T., "The Transient Ground Surface Displacements Due to a Point Sink/Heat Source in an Elastic Half-space," *Geotechnical Special Publication No. 148*, *ISBN 0-7844-0860-2, GeoShanghai International Conference 2006, ASCE*, pp. 210-218, 2006.
8. Lu, J. C.-C. and Lin, F.-T. "Thermo-consolidation Due to a Point Heat Source Buried in a Poroelastic Half Space," *Proceedings of the 3rd IASTED International Conference on Environmental Modelling and Simulation*, Honolulu, Hawaii, U.S.A., pp. 48-53, August 20~22, 2007.
9. Lu, J. C.-C., "Long-Term Behaviors of a Buried Deep Point Heat Source in a Transversely Isotropic Thermoelastic Porous Medium," *Chung Hua Journal of Science and Engineering*, Vol. 4, No. 1, pp. 11-22, 2006.
10. Lin, F.-T. and Lu, John C.-C., "Analysis of Transient Ground Surface Displacements Due to an Instantaneous Point Heat Source," *Proceedings of the 20th IASTED International Conference on Modelling and Simulation*, Banff, Alberta, Canada, pp. 57-64, July 6~8, 2009.

11. Gradshteyn, I.S. and Ryzhik, I.M., *Table of Integrals, Series, and Products*, 4th Edition, Academic Press, New York, 1160p, 1980.

符號說明

c	Parameter, $c = \lambda_t / c_\varepsilon$ (m^2/s); Specific heat of the stratum at a constant deformation $(J/kg^\circ C)$
c_ε	Parameter, $c_\varepsilon = \rho c$ $(J/m^3{}^\circ C)$
$erfc(x)$	Complementary error function (Dimensionless)
G	Shear modulus of the isotropic stratum (Pa)
h	Buried depth of the point heat source (m)
$J_\nu(x)$	First kind of the Bessel function of order ν (Dimensionless)
$q(r,z,t)$	The concentrated thermal loading rate $(1/s)$
$\tilde{q}(z;\xi,s)$	Laplace and Hankel transformations of $q(r,z,t)$ $(1/m^2s^2)$
Q_0	Thermal strength generated by the point heat source (J)
Q_c	Strength of the point heat source generated at a constant rate (J/s)
(r,θ,z)	Cylindrical coordinates system $(m, radian, m)$
s	Laplace transform parameter (s^{-1})
t	Time (s)
$u(t)$	Heaviside unit step function (Dimensionless)
u_r	Horizontal displacement of the stratum (m)
u_z	Vertical displacement of the stratum (m)
α_s	Linear thermal expansion coefficient $(1/^\circ C)$
β	Thermal parameter, $\beta = (2G + 3\lambda)\alpha_s$ $(Pa/^\circ C)$
$\delta(r)$	Dirac delta function (m^{-1})
$\delta(t)$	Dirac delta function (s^{-1})
$\delta(z-h)$	Dirac delta function (m^{-1})
ε	Volume strain of the stratum (Dimensionless)
η	Parameter, $\eta = (1-\nu)/(1-2\nu)$ (Dimensionless)
$\vartheta(r,z,t)$	Temperature increment of the stratum $(^\circ C)$
$\tilde{\vartheta}(z;\xi,s)$	Laplace and Hankel transformations of $\vartheta(r,z,t)$ $(^\circ C/sm^2)$
λ_t	Thermal conductivity of the stratum $(J/ms^\circ C)$
ν	Poisson's ratio of the isotropic stratum (Dimensionless)

ξ	Hankel transform parameter (m^{-1})
ρ	Mass density of the stratum (kg/m^3)
τ_{ij}	Thermal stress components of the stratum (Pa)
∇^2	Differential operator, $\nabla^2 = \partial^2/\partial r^2 + 1/r\,\partial/\partial r + \partial^2/\partial z^2$ $(1/m^2)$

3-3 深層點熱源所引致橫向等向性地層之熱彈性行為的解析

ABSTRACT
The deep point heat source affects long-term thermal responses of an elastic soil mass. To simulate the stratified earth medium, the soil mass is modeled as a cross-anisotropic thermoelastic medium with different properties in horizontal and vertical directions. Analytical solutions of the displacements and temperature imcrements of the soils are obtained by using Hankel integral transform. Numerical results for thermal stresses are presented to portray the effects of anisotropic thermal properties on the response of a point heat source. The rise of the ratio of linear thermal expansion coefficients α_{sr}/α_{sz} leads to corresponding rise of thermal stress components with varying degrees of anisotropy. However, the thermal stress components decrease with increase of the ratio of the thermal conductivities $\lambda_{tr}/\lambda_{tz}$.

KEY WORDS
Mathematical Modelling, 3-Dimensional Modelling, Point Heat Source, Closed-form Solution

1. Introduction

Heat source placed at a great depth leads to thermo-mechanical responses of the stratum. The heat source such as a canister of radioactive waste can cause temperature rise in the soil. This leads to a reduction in soil stresses. Therefore, thermal failure of soil will occur as a result of losing shear resistance.

Repositories of nuclear waste are usually designed at a depth of 200-700 m below the ground surface [1]. At such great depths, soil is in the state of full saturation with no air fraction. Also, water cannot vaporize at temperatures below 150°*C* due to high water pressure at such depth. Heremans *et al.* [2] confirmed this hypothesis through an experiment consisting simulation of heating at such conditions.

Attention of this paper is focused on the closed-form solutions of a cross-anisotropic stratum due to a deep point heat source. The behavior of the soil was satisfactorily modeled by assuming as a thermoelastic continuum [3]. It suggested that linear theory was adequate for a repository design based on technical conservatism. For example, Hueckel and Peano [4] indicated that European guidelines require that temperature increments in the soil close to the heat source should not exceed 80°*C* while the temperature increments at the ground surface is limited to less than 1°*C*. Given these modest temperature increments, Hollister *et al.* [5] observed that any significant non-linear behavior and/or plastic deformation of the soil would be confined to a relatively small volume of soil around the waste canister itself. In this case, a linear model can provide a reasonable approximation to the assessment of a proposed design [6].

Booker and Savvidou [3,7], Savvidou and Booker [8] derived an extended Biot [9,10] theory including the thermal effects and presented solutions of thermo-consolidation around the spherical and point heat sources. In their solutions, the flow properties are considered as isotropic or cross-anisotropic, whereas the elastic and thermal properties of the soils are treated as isotropic. Lu and Lin [11] displayed transient ground surface displacement produced by a point heat source/sink through analog quantities between poroelasticity and thermoelasticity. Based on Biot's three-dimensional consolidation theory of porous media, analytical solutions of the transient thermo-consolidation deformation due to a point heat source buried in a saturated isotropic porous elastic half space were presented by Lu and Lin [12,13]. Nevertheless, the above studies did not include thermoelastic responses of the stratum with cross-anisotropic thermal flow properties corresponding to the isotropic mechanical properties due to a point heat source.

The soils are generally deposited through a process of sedimentation over a long period of time. Under accumulative overburden pressure, soils display significant anisotropy for thermal properties. To describe the anisotropic nature of soils, it is modeled as a cross-anisotropic medium whose properties are symmetric in vertical axis. If the heat source is buried at a great depth, the effects of the ground surface boundary on thermo-mechanical responses of the stratum can be neglected.

In this study, the soil mass is modeled as a cross-anisotropic thermoelastic full space. Cross-anisotropic thermal conductivity is considered in this study. Long-term thermoelastic responses of soils are derived through Hankel transform. The closed-form solutions of thermoelastic deformation, temperature increments of the soil mass and thermal stresses of the stratum due to a point heat source are evaluated. A simplified example of isotropic soil is examined to provide better understanding of the thermally induced mechanical problem.

2. Mathematical Model

2.1 Basic Equations

The soil mass is considered as a homogeneous cross-anisotropic full space with a vertical axis of symmetry. The thermal properties of the stratum are treated as cross-anisotropic while the mechanical properties of the soils are modeled as isotropic in this study. Therefore, the

constitutive behavior of the thermoelastic soil skeleton for linear axisymmetric deformation in the cylindrical coordinates (r,θ,z) is:

$$\sigma_{rr}=\frac{2G(1-\nu)}{1-2\nu}\frac{\partial u_r}{\partial r}+\frac{2G\nu}{1-2\nu}\frac{u_r}{r}+\frac{2G\nu}{1-2\nu}\frac{\partial u_z}{\partial z}-\beta_r\vartheta, \quad (1a)$$

$$\sigma_{\theta\theta}=\frac{2G\nu}{1-2\nu}\frac{\partial u_r}{\partial r}+\frac{2G(1-\nu)}{1-2\nu}\frac{u_r}{r}+\frac{2G\nu}{1-2\nu}\frac{\partial u_z}{\partial z}-\beta_r\vartheta, \quad (1b)$$

$$\sigma_{zz}=\frac{2G\nu}{1-2\nu}\frac{\partial u_r}{\partial r}+\frac{2G\nu}{1-2\nu}\frac{u_r}{r}+\frac{2G(1-\nu)}{1-2\nu}\frac{\partial u_z}{\partial z}-\beta_z\vartheta, \quad (1c)$$

$$\sigma_{rz}=G\left(\frac{\partial u_r}{\partial z}+\frac{\partial u_z}{\partial r}\right), \quad (1d)$$

where σ_{rr} , $\sigma_{\theta\theta}$, σ_{zz} and σ_{rz} are the thermal stress components. The quantity ϑ measures the temperature increment of the soil mass. The variables u_r and u_z are displacements in the radial and axial directions, respectively. The parameters G and ν are the shear modulus and Poisson's ratio of the solid skeleton, respectively. The thermal expansion factors β_r and β_z in horizontal and vertical directions, respectively, are defined as:

$$\beta_r=2G(\alpha_{sr}+\nu\alpha_{sz})/(1-2\nu), \quad (2a)$$

$$\beta_z=2G[2\nu\alpha_{sr}+(1-\nu)\alpha_{sz}]/(1-2\nu), \quad (2b)$$

where the coefficients α_{sr} and α_{sz} are the linear thermal expansion coefficient of the skeletal material in the horizontal and vertical directions, respectively. The shear stress components $\sigma_{r\theta}$ and $\sigma_{\theta z}$ vanish with a vertical axis of symmetry. For an isotropic thermoelastic medium, the thermal expansion factors became $\beta_r=\beta_z=\beta=(2G+3\lambda)\alpha_s$. Here, λ is the Lame constant of the isotropic soil mass and α_s denotes the linear thermal expansion coefficient of the isotropic soil skeleton.

The thermal stresses σ_{ij} must satisfy the following equilibrium relations:

$$\sigma_{ij,j}+b_i=0, \quad (3)$$

where b_i denote the body forces. By equations (1a)-(1d), the equilibrium equations for axisymmetric deformation with vanishing body forces $(b_i=0)$ can be expressed in terms of displacements u_i and temperature increment of the soil mass ϑ as below:

$$G\nabla^2u_r+\frac{G}{1-2\nu}\frac{\partial\varepsilon}{\partial r}-G\frac{u_r}{r^2}-\beta_r\frac{\partial\vartheta}{\partial r}=0, \quad (4a)$$

$$G\nabla^2u_z+\frac{G}{1-2\nu}\frac{\partial\varepsilon}{\partial z}-\beta_z\frac{\partial\vartheta}{\partial z}=0, \quad (4b)$$

where $\nabla^2=\partial^2/\partial r^2+1/r\,\partial/\partial r+\partial^2/\partial z^2$ is the differential operator. The volume strain $\varepsilon=\partial u_r/\partial r+u_r/r+\partial u_z/\partial z$.

Besides of equations (4a) and (4b), another equation for the three variables u_r , u_z and ϑ are obtained from the conservation of energy:

$$-\nabla\cdot\boldsymbol{h}+q_h=0, \quad (5)$$

where $\boldsymbol{h}$ and q_h are the heat flux vector and internal/external heat source, respectively.

The anisotropic thermal flow is assumed to be governed by Fourier's law as follows:

$$\boldsymbol{h}=-\lambda_{tr}\frac{\partial\vartheta}{\partial r}\boldsymbol{i}_r-\lambda_{tz}\frac{\partial\vartheta}{\partial z}\boldsymbol{i}_z, \quad (6)$$

where the quantities λ_{tr} and λ_{tz} are the thermal conductivities of soil mass in the horizontal and vertical directions, respectively. The symbols $\boldsymbol{i}_r$ and $\boldsymbol{i}_z$ denote the unit vectors parallel to the radial and vertical directions, respectively.

Let us consider a deep point heat source of constant strength Q located at the position of $(0,0)$ and substituting (6) into (5) lead to

$$\lambda_{tr}\left(\frac{\partial^2\vartheta}{\partial r^2}+\frac{1}{r}\frac{\partial\vartheta}{\partial r}\right)+\lambda_{tz}\frac{\partial^2\vartheta}{\partial z^2}+\frac{Q}{2\pi r}\delta(r)\delta(z)=0, \quad (7)$$

where $\delta(x)$ is the Dirac delta function. Equations (4a), (4b) and (7) constitute the basic governing equations of the axisymmetric thermally elastic responses of a cross-anisotropic stratum subjected to a deep point heat source.

2.2 Boundary Conditions

It's reasonable to assume that the effect of point heat source vanishes at infinity ($z\to\pm\infty$). Therefore, the boundary conditions for the full space are represented as:

$$\lim_{z\to\pm\infty}\{u_r(r,z),u_z(r,z),\vartheta(r,z)\}=\{0,0,0\}. \quad (8)$$

The basic equations (4a), (4b), (7) and corresponding boundary conditions (8) constitute the mathematical model of the presented study.

3. Analytic Solution

The closed-form solutions of thermoelastic deformation, temperature change of the soil mass and thermal stresses

due to a point heat source buried in a cross-anisotropic elastic full space can be obtained by using Hankel transform [14] and equations (1a)-(1d) as follows:

$$u_r = \frac{Q\alpha_{sz}}{4\pi\eta\lambda_{tz}}\left\{\beta_r^*\phi_1(r,z) + \left[2\eta\beta_r^* - (2\eta-1)\beta_z^*\right]\phi_2(r,z)\right\}, \tag{9a}$$

$$u_z = \frac{Q\alpha_{sz}}{4\pi\eta\lambda_{tz}}\left\{\beta_z^*\phi_3(r,z) + \left[2\eta\beta_z^* - (2\eta-1)\beta_r^*\right]\phi_4(r,z)\right\}, \tag{9b}$$

$$\vartheta = \frac{Q}{4\pi\lambda_{tz}}\phi_5(r,z), \tag{9c}$$

$$\sigma_{rr} = \frac{QG\alpha_{sz}}{4\pi\eta\lambda_{tz}}\left\{(2\eta-1)\beta_r^*\phi_6(r,z) + 2(\eta-1)\beta_z^*\phi_7(r,z) + \left[2(2\eta-1)\beta_r^* - \beta_z^*\right]\phi_8(r,z) + \eta\beta_r^*\phi_9(r,z) + \beta_r^*\phi_{10}(r,z) + \left[2\eta\beta_r^* - (2\eta-1)\beta_z^*\right]\phi_{11}(r,z)\right\}, \tag{9d}$$

$$\sigma_{\theta\theta} = \frac{QG\alpha_{sz}}{4\pi\eta\lambda_{tz}}\left\{(2\eta-1)\beta_r^*\phi_6(r,z) + 2(\eta-1)\beta_z^*\phi_7(r,z) + \left[2(2\eta-1)\beta_r^* - \beta_z^*\right]\phi_8(r,z) + \eta\beta_r^*\phi_9(r,z) - \beta_r^*\phi_{10}(r,z) - \left[2\eta\beta_r^* - (2\eta-1)\beta_z^*\right]\phi_{11}(r,z)\right\}, \tag{9e}$$

$$\sigma_{zz} = \frac{QG\alpha_{sz}}{4\pi\eta\lambda_{tz}}\left\{2(\eta-1)\beta_r^*\phi_6(r,z) + 2\eta\beta_z^*\phi_7(r,z) + \left[-2\eta\beta_r^* + 2(3\eta-1)\beta_z^*\right]\phi_8(r,z) + \eta\beta_z^*\phi_9(r,z)\right\}, \tag{9f}$$

$$\sigma_{rz} = \frac{QG\alpha_{sz}}{4\pi\eta\lambda_{tz}}\left\{\left[2\eta\beta_r^* - 2(\eta-1)\beta_z^*\right]\phi_{12}(r,z) + \left[2\eta\beta_z^* - 2(\eta-1)\beta_r^*\right]\phi_{13}(r,z)\right\}, \tag{9g}$$

where $\eta = (1-\nu)/(1-2\nu)$. The parameters β_r^* and β_z^* are defined as follows:

$$\beta_r^* = 2(\nu + \alpha_{sr}/\alpha_{sz})/(1-2\nu), \tag{10a}$$

$$\beta_z^* = 2\left[(1-\nu) + 2\nu\,\alpha_{sr}/\alpha_{sz}\right]/(1-2\nu). \tag{10b}$$

The definitions of functions $\phi_i\,(i=1,\cdots,13)$ in (9a)-(9g) are listed below:

$$\phi_1(r,z) = \frac{1}{4(\mu^2-1)}\frac{r}{R} - \frac{1}{2(\mu^2-1)^2}\frac{r}{R^*} + \frac{1}{2\mu(\mu^2-1)^2}\frac{r}{R_\mu^*}, \tag{11a}$$

$$\phi_2(r,z) = \frac{1}{4(\mu^2-1)}\left(-\frac{r|z|}{RR^*} + \frac{r}{R^*}\right) + \frac{1}{2(\mu^2-1)^2}\frac{r}{R^*} - \frac{\mu}{2(\mu^2-1)^2}\frac{r}{R_\mu^*}, \tag{11b}$$

$$\phi_3(r,z) = -\frac{1}{4(\mu^2-1)}\frac{z}{R} - \frac{\mu^2}{2(\mu^2-1)^2}\sinh^{-1}\frac{z}{r} + \frac{\mu^2}{2(\mu^2-1)^2}\sinh^{-1}\frac{\mu z}{r}, \tag{11c}$$

$$\phi_4(r,z) = \frac{1}{4(\mu^2-1)}\frac{z}{R} + \frac{1}{2(\mu^2-1)^2}\sinh^{-1}\frac{z}{r} - \frac{1}{2(\mu^2-1)^2}\sinh^{-1}\frac{\mu z}{r}, \tag{11d}$$

$$\phi_5(r,z) = \frac{1}{\mu R_\mu}, \tag{11e}$$

$$\phi_6(r,z) = \frac{1}{4(\mu^2-1)}\left(\frac{1}{R} + \frac{z^2}{R^3}\right) - \frac{1}{2(\mu^2-1)^2}\frac{1}{R} + \frac{1}{2\mu(\mu^2-1)^2}\frac{1}{R_\mu}, \tag{11f}$$

$$\phi_7(r,z) = \frac{1}{4(\mu^2-1)}\left(-\frac{3}{R} + \frac{z^2}{R^3}\right) - \frac{1}{2(\mu^2-1)^2}\frac{1}{R} + \frac{\mu^3}{2(\mu^2-1)^2}\frac{1}{R_\mu}, \tag{11g}$$

$$\phi_8(r,z) = \frac{1}{4(\mu^2-1)}\frac{r^2}{R^3} + \frac{1}{2(\mu^2-1)^2}\frac{1}{R} - \frac{\mu}{2(\mu^2-1)^2}\frac{1}{R_\mu}, \tag{11h}$$

$$\phi_9(r,z) = -\frac{1}{\mu R_\mu}, \tag{11i}$$

$$\phi_{10}(r,z) = -\frac{1}{4(\mu^2-1)}\frac{r^2}{R^3} + \frac{1}{2(\mu^2-1)^2}\frac{r^2}{RR^{*2}} - \frac{1}{2\mu(\mu^2-1)^2}\frac{r^2}{R_\mu R_\mu^{*2}}, \tag{11j}$$

$$\phi_{11}(r,z) = \frac{1}{4(\mu^2-1)}\frac{r^2}{R^3} - \frac{\mu^2}{2(\mu^2-1)^2}\frac{r^2}{RR^{*2}} + \frac{\mu}{2(\mu^2-1)^2}\frac{r^2}{R_\mu R_\mu^{*2}}, \tag{11k}$$

$$\phi_{12}(r,z) = \frac{1}{4(\mu^2-1)}\frac{rz}{R^3} - \frac{\mu^2}{2(\mu^2-1)^2}\frac{r}{RR^*}$$

$$+\frac{\mu^2}{2\left(\mu^2-1\right)^2}\frac{r}{R_\mu R_\mu^*}, \tag{11l}$$

$$\phi_{13}(r,z)=-\frac{1}{4\left(\mu^2-1\right)}\frac{rz}{R^3}+\frac{1}{2\left(\mu^2-1\right)^2}\frac{r}{RR^*}$$

$$-\frac{1}{2\left(\mu^2-1\right)^2}\frac{r}{R_\mu R_\mu^*}, \tag{11m}$$

in which the parameters $\mu=\sqrt{\lambda_{tr}/\lambda_{tz}}$, $R=\sqrt{r^2+z^2}$, $R^*=\sqrt{r^2+z^2}+|z|$, $R_\mu=\sqrt{r^2+\mu^2z^2}$, and $R_\mu^*=\sqrt{r^2+\mu^2z^2}+\mu|z|$, respectively.

Using L'Hospital's rule and applying the limit $\lambda_{tr}/\lambda_{tz}\to 1$ and $\alpha_{sr}/\alpha_{sz}\to 1$, the solutions of an isotropic soil mass with isotropic heat conductivity are obtained from (9a)-(9g). Carrying out the procedure, we obtain

$$u_r=\frac{Q\alpha_s(1+\nu)}{8\pi\lambda_t(1-\nu)}\frac{r}{R}, \tag{12a}$$

$$u_z=\frac{Q\alpha_s(1+\nu)}{8\pi\lambda_t(1-\nu)}\frac{z}{R}, \tag{12b}$$

$$\vartheta=\frac{Q}{4\pi\lambda_t}\frac{1}{R}, \tag{12c}$$

$$\sigma_{rr}=-\frac{QG\alpha_s(1+\nu)}{4\pi\lambda_t(1-\nu)}\left(\frac{1}{R}+\frac{r^2}{R^3}\right), \tag{12d}$$

$$\sigma_{\theta\theta}=-\frac{QG\alpha_s(1+\nu)}{4\pi\lambda_t(1-\nu)}\frac{1}{R}, \tag{12e}$$

$$\sigma_{zz}=-\frac{QG\alpha_s(1+\nu)}{4\pi\lambda_t(1-\nu)}\left(\frac{1}{R}+\frac{z^2}{R^3}\right), \tag{12f}$$

$$\sigma_{rz}=-\frac{QG\alpha_s(1+\nu)}{4\pi\lambda_t(1-\nu)}\frac{rz}{R^3}, \tag{12g}$$

where λ_t denotes thermal conductivity of the isotropic soils.

From the derived closed-form solutions, equations (9a)-(9g), we find all field quantities are functions of the distance from the heat source and are proportional to the linear thermal expansion coefficient. However, they are inversely proportional to the thermal conductivity. Besides, the shear modulus does not have influence on displacements and temperature increment of the soils.

4. Numerical Results

Referring to the soil element in Figure 1, the numerical results of the thermal stress distributions of σ_{ij} are summarized in Figures 2-5. The assumed Poisson's ratio of the soil mass is $\nu=0.3$, and the thermal stresses were normalized by the factor $QG\alpha_{sz}/4\pi\lambda_{tz}$. As shown in the figures 2-5, the isobaric contours of thermal stresses of soil mass σ_{rr}, $\sigma_{\theta\theta}$, σ_{zz} and σ_{rz} near the point heat source are significantly affected by the ratio of thermal properties α_{sr}/α_{sz} and $\lambda_{tr}/\lambda_{tz}$. The rise of the ratio of linear thermal expansion coefficients α_{sr}/α_{sz} leads to corresponding rise of thermal stress components with varying degrees of anisotropy. Nevertheless, the thermal stress components decrease with the increase of the ratio of thermal conductivities $\lambda_{tr}/\lambda_{tz}$. All thermal stress changes are compressive, and it helps to prevent thermal failure of soil.

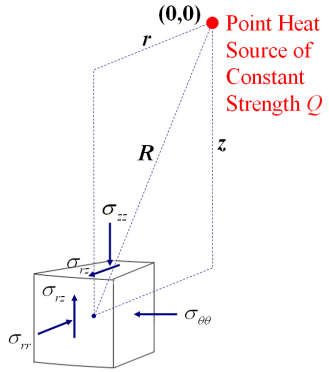

Figure 1. Thermal stresses on soil element due to a deep point heat source.

High-level radioactive waste generates heat, and it leads to temperature increase for the soil surrounding the canister. Hueckel and Peano [4] indicated that European guidelines require that temperature increments in the soil close to the heat source should not exceed $80°C$ while the temperature increments at the ground surface is limited to less than $1°C$. The heat outputs generated by canisters are assumed to be 224 *W/m* [15], 325 *W/m* [1], or 1000 *W/m* [6].

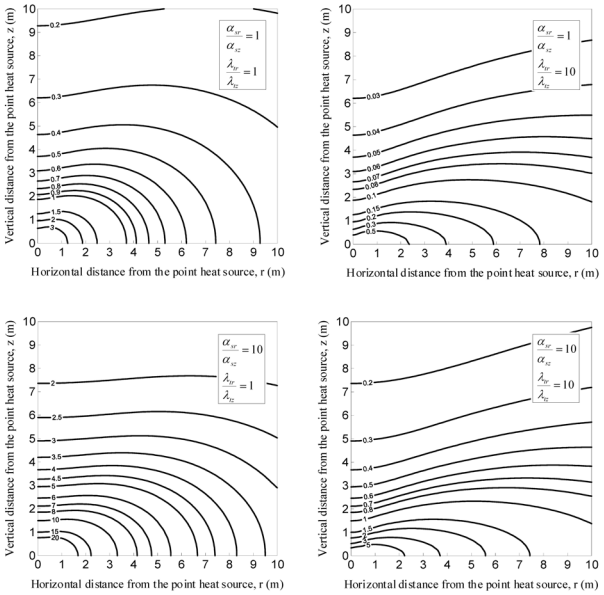

Figure 2. Isobaric contours of normalized thermal stress $-\sigma_{rr}/\left[QG\alpha_{sz}/4\pi\lambda_{tz}\right]$ due to a point heat source for different ratios of α_{sr}/α_{sz} and $\lambda_{tr}/\lambda_{tz}$.

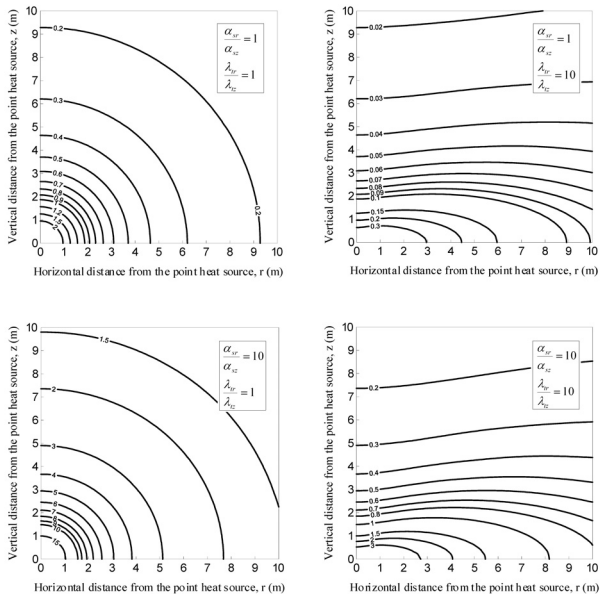

Figure 3. Isobaric contours of normalized thermal stress $-\sigma_{\theta\theta}/\left[QG\alpha_{sz}/4\pi\lambda_{tz}\right]$ due to a point heat source for different ratios of α_{sr}/α_{sz} and $\lambda_{tr}/\lambda_{tz}$.

On the basis of equations (12a)-(12g), Tables 1 and 2 gives the normalized values of the derived analytical solutions. The selected representative parameters of isotropic soil, Boom clay, are listed in Table 3 to verify the proposed solutions.

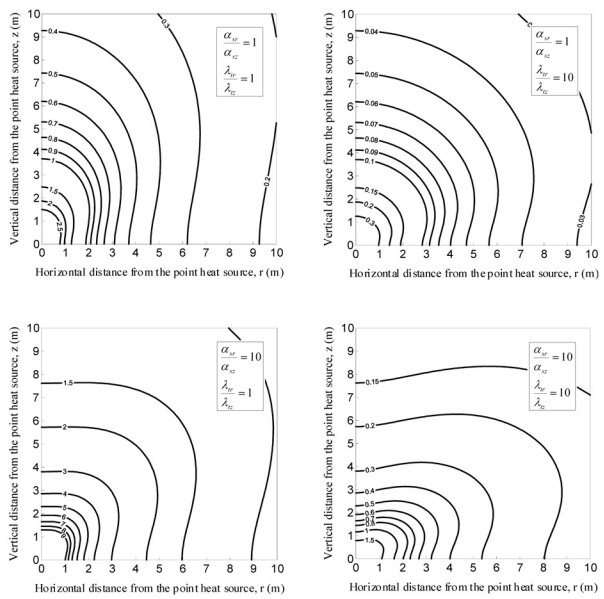

Figure 4. Isobaric contours of normalized thermal stress $-\sigma_{zz}/\left[QG\alpha_{sz}/4\pi\lambda_{tz}\right]$ due to a point heat source for different ratios of α_{sr}/α_{sz} and $\lambda_{tr}/\lambda_{tz}$.

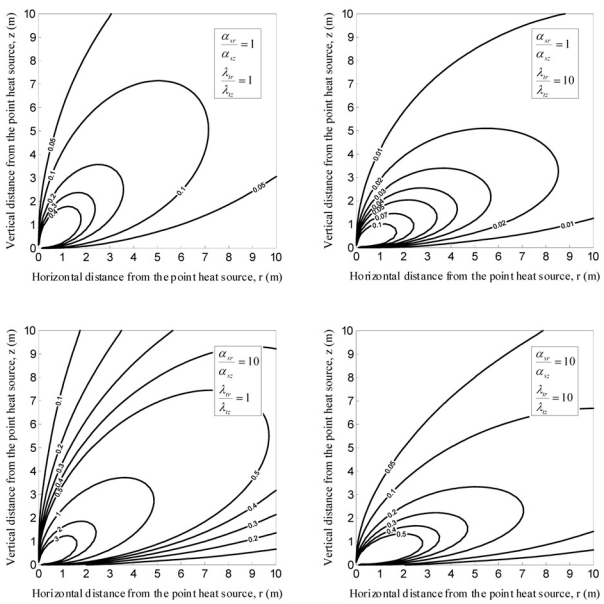

Figure 5. Isobaric contours of normalized thermal stress $-\sigma_{rz}/\left[QG\alpha_{sz}/4\pi\lambda_{tz}\right]$ due to a point heat source for different ratios of α_{sr}/α_{sz} and $\lambda_{tr}/\lambda_{tz}$.

At the distance of r = 0~10 *m* and z = 0.3 *m* away from the heat source corresponding to the parameters listed in Table 3, the displacements, temperature increments and thermal stresses of the stratum due to a deep point heat source are shown in Tables 4 and 5, respectively.

Table 1. Normalized values of the displacements and temperature change of the isotropic soil due to a deep point heat source.

$\frac{r}{z}$	$\frac{u_r}{\frac{Q\alpha_s(1+\nu)}{8\pi\lambda_t(1-\nu)}}$	$\frac{u_z}{\frac{Q\alpha_s(1+\nu)}{8\pi\lambda_t(1-\nu)}}$	$\frac{\vartheta}{\frac{Q}{4\pi\lambda_t z}}$
0.0	0.0000	1.0000	1.0000
1.0	0.7071	0.7071	0.7071
2.0	0.8944	0.4472	0.4472
3.0	0.9487	0.3162	0.3162
4.0	0.9701	0.2425	0.2425
5.0	0.9806	0.1961	0.1961
6.0	0.9864	0.1644	0.1644
7.0	0.9899	0.1414	0.1414
8.0	0.9923	0.1240	0.1240
9.0	0.9939	0.1104	0.1104
10.0	0.9950	0.0995	0.0995

Table 2. Normalized values of the thermal stresses of the isotropic soil due to a deep point heat source.

$\frac{r}{z}$	$\frac{-\sigma_{rr}}{\frac{QG\alpha_s(1+\nu)}{4\pi\lambda_t(1-\nu)z}}$	$\frac{-\sigma_{\theta\theta}}{\frac{QG\alpha_s(1+\nu)}{4\pi\lambda_t(1-\nu)z}}$	$\frac{-\sigma_{zz}}{\frac{QG\alpha_s(1+\nu)}{4\pi\lambda_t(1-\nu)z}}$	$\frac{-\sigma_{rz}}{\frac{QG\alpha_s(1+\nu)}{4\pi\lambda_t(1-\nu)z}}$
0.0	1.0000	1.0000	2.0000	0.0000
1.0	1.0607	0.7071	1.0607	0.3536
2.0	0.8050	0.4472	0.5367	0.1789
3.0	0.6008	0.3162	0.3479	0.0949
4.0	0.4708	0.2425	0.2568	0.0571
5.0	0.3847	0.1961	0.2037	0.0377
6.0	0.3244	0.1644	0.1688	0.0267
7.0	0.2800	0.1414	0.1442	0.0198
8.0	0.2462	0.1240	0.1259	0.0153
9.0	0.2195	0.1104	0.1118	0.0121
10.0	0.1980	0.0995	0.1005	0.0099

Table 3. Selected representative parameters [1].

Parameter	Symbol	Value	Units
Shear modulus	G	100	MN/m^2
Thermal strength	Q	325	J/s
Linear thermal expansion coefficient	α_s	1.17×10^{-4}	$°C^{-1}$
Thermal conductivity	λ_t	1.69	$J/sm°C$
Poisson's ratio	ν	0.35	Dimensionless

Note: The thermal strength Q that simulates the high-level radioactive waste is obtained from an assumed 1 m length line heat source with the heat output strength of 325 W/m.

Table 4. Typical values of the displacements and temperature increments of the isotropic soil due to a deep point heat source.

r (m)	z (m)	u_r (m)	u_z (m)	ϑ $(°C)$
0.0	0.3	0.000000	0.001859	51.0
0.1	0.3	0.000588	0.001764	48.4
0.2	0.3	0.001031	0.001547	42.4
0.3	0.3	0.001315	0.001315	36.1
1.0	0.3	0.001781	0.000534	14.7
2.0	0.3	0.001839	0.000276	7.6
3.0	0.3	0.001850	0.000185	5.1
4.0	0.3	0.001854	0.000139	3.8
5.0	0.3	0.001856	0.000111	3.1
6.0	0.3	0.001857	0.000093	2.5
7.0	0.3	0.001858	0.000080	2.2
8.0	0.3	0.001858	0.000070	1.9
9.0	0.3	0.001858	0.000062	1.7
10.0	0.3	0.001859	0.000056	1.5

Table 5. Typical values of the thermal stresses of the isotropic soil due to a deep point heat source.

r (m)	z (m)	σ_{rr} (Pa)	$\sigma_{\theta\theta}$ (Pa)	σ_{zz} (Pa)	σ_{rz} (Pa)	$\frac{\sigma_{rr}}{\sigma_{zz}}$	$\frac{\sigma_{\theta\theta}}{\sigma_{zz}}$
0.0	0.3	-1,239,572	-1,239,572	-2,479,144	0	0.50	0.50
0.1	0.3	-1,293,558	-1,175,961	-2,234,327	-352,788	1.77	0.92
0.2	0.3	-1,348,736	-1,031,386	-1,745,423	-476,024	1.77	0.92
0.3	0.3	-1,314,765	-876,510	-1,314,765	-438,255	1.77	0.92
1.0	0.3	-682,967	-356,188	-385,598	-98,034	1.77	0.92
2.0	0.3	-363,711	-183,879	-187,925	-26,975	1.94	0.98
3.0	0.3	-245,463	-123,342	-124,563	-12,212	1.97	0.99
4.0	0.3	-184,897	-92,708	-93,226	-6,914	1.98	0.99
5.0	0.3	-148,215	-74,241	-74,507	-4,438	1.99	1.00
6.0	0.3	-123,648	-61,901	-62,056	-3,087	1.99	1.00
7.0	0.3	-106,054	-53,076	-53,173	-2,271	1.99	1.00
8.0	0.3	-92,837	-46,451	-46,517	-1,739	2.00	1.00
9.0	0.3	-82,546	-41,296	-41,342	-1,375	2.00	1.00
10.0	0.3	-74,307	-37,170	-37,204	-1,114	2.00	1.00

The maximum radial displacement u_r, vertical displacement u_z, temperature increment ϑ, radial normal stress σ_{rr}, hoop normal stress $\sigma_{\theta\theta}$, vertical normal stress σ_{zz} and shear stress σ_{rz} of the stratum shown in Tables 4 and 5 are 1.859 mm, 1.859 mm, 51°C, -1.35 MPa, -1.24 MPa, -2.48 MPa and -0.48 MPa, respectively. The temperature increment is below 1°C at the soil stratum 16 m away from the point heat source. The ratio of the radial normal stress σ_{rr} to the vertical normal stress σ_{zz} ranges from 0.5 to 2.0, and the ratio of the hoop normal stress $\sigma_{\theta\theta}$ to the vertical normal stress σ_{zz} ranges from 0.5 to 1.0.

5. Conclusions

The closed-form solutions of thermoelastic responses due to a point heat source buried in a cross-anisotropic thermoelastic full space were obtained by using Hankel transform. The results were examined by simplifying the solutions of cross-anisotropic thermoelastic responses into the case of isotropic one. The solutions show that:

1. All field quantities are functions of the distance from the heat source and are proportional to the linear thermal expansion coefficient. However, they are inversely proportional to the thermal conductivity. Besides, the shear modulus does not have influence on displacements and temperature increment of the soils.
2. Based on the numerical results obtained for the anisotropic thermoelastic study, the thermal stresses of soil mass are compressive and are significantly affected by the ratio of thermal properties α_{sr}/α_{sz} and $\lambda_{tr}/\lambda_{tz}$. The rise of the ratio of linear thermal expansion coefficients α_{sr}/α_{sz} leads to corresponding rise of thermal stress components with varying degrees of anisotropy. However, the thermal stress components decrease with increase of the ratio of the thermal conductivities $\lambda_{tr}/\lambda_{tz}$.
3. At the distance of r = 0~10 m and z = 0.3 m away from the heat source corresponding to the parameters listed in Table 3, we obtained the ratio of the radial normal stress σ_{rr} to the vertical normal stress σ_{zz} ranges from 0.5 to 2.0, and the ratio of the hoop normal stress $\sigma_{\theta\theta}$ to the vertical normal stress σ_{zz} ranges from 0.5 to 1.0.

Acknowledgements

This work is supported by the National Science Council of Republic of China through grant NSC-98-2815-C-216-007-E, and also by the Chung Hua University under grant CHU-98-2815-C-216-007-E.

References

[1] C. Ma & T. Hueckel, Stress and pore pressure in saturated clay subjected to heat from radioactive waste: a numerical simulation, *Canadian Geotechnical Journal*, 29, 1992, 1087-1094.

[2] R.H. Heremans, A. Barbreau, P. Bourke & H. Gies, Thermal aspects associated with the disposal of waste in deep geological formations, In *Radioactive waste management and disposal*, Edited by R. Simon and S. Orlowski, 468-487 (London, Harwood Academic Publishers: 1980).

[3] J.R. Booker & C. Savvidou, Consolidation around a point heat source, *International Journal for Numerical and Analytical Methods in Geomechanics*, 9(2), 1985, 173-184.

[4] T. Hueckel & A. Peano, Some geotechnical aspects of radioactive waste isolation in continental clays, *Computers and Geotechnics*, 3, 1987, 157-182.

[5] C.D. Hollister, D.R. Anderson & G.R. Heath, Seabed disposal of nuclear wastes, *Science*, 213(4514), 1981, 1321-1326.

[6] D.W. Smith & J.R. Booker, Boundary element analysis of linear thermoelastic consolidation, *International Journal for Numerical and Analytical Methods in Geomechanics*, 20, 1996, 457-488.

[7] J.R. Booker & C. Savvidou, Consolidation around a spherical heat source, *International Journal of Solids and Structures*, 20(11/12), 1984, 1079-1090.

[8] C. Savvidou & J.R. Booker, Consolidation around a heat source buried deep in a porous thermoelastic medium with anisotropic flow properties, *International Journal for Numerical and Analytical Methods in Geomechanics*, 13(1), 1989, 75-90.

[9] M.A. Biot, General theory of three-dimensional consolidation, *Journal of Applied Physics*, 12(2), 1941, 155-164.

[10] M.A. Biot, Theory of elasticity and consolidation for a porous anisotropic solid, *Journal of Applied Physics*, 26(2), 1955, 182-185.

[11] J. C.-C. Lu & F.-T. Lin, The transient ground surface displacements due to a point sink/heat source in an elastic half-space, *Geotechnical Special Publication No. 148*, *ASCE*, 2006, 210-218.

[12] J. C.-C. Lu & F.-T. Lin, Thermo-consolidation due to a point heat source buried in a poroelastic half space, *Proceedings of the 3rd IASTED International Conference on Environmental Modelling and Simulation*, Honolulu, Hawaii, U.S.A., 2007, 48-53.

[13] F.-T. Lin & J. C.-C. Lu, Analysis of transient ground surface displacements due to an instantaneous point heat source, *Proceedings of the 20th IASTED International Conference on Modelling and Simulation*, Banff, Alberta, Canada, 2009, 59-64.

[14] I.N. Sneddon, *Fourier transforms* (New York: McGraw-Hill, 1951, 48-70).

[15] C. Ma & T. Hueckel, Thermomechanical effects on adsorbed water in clays around a heat source,

International Journal for Numerical and Analytical Methods in Geomechanics, 17, 1993, 175-196.

Nomenclature

b_i Body forces (*Pa*/*m*)

G Shear modulus of the isotropic thermoelastic medium (*Pa*)

$\boldsymbol{h}$ Heat flux vector (J/sm^2)

$\boldsymbol{i}_r/\boldsymbol{i}_z$ Unit vector parallel to the radial/vertical direction (Dimensionless)

q_h Internal/external heat source (J/sm^3)

Q Strength of the point heat source (*J*/*s*)

(r,θ,z) Cylindrical coordinates system (*m*, *radian*, *m*)

R Parameter, $R=\sqrt{r^2+z^2}$ (*m*)

R^* Parameter, $R^*=\sqrt{r^2+z^2}+|z|$ (*m*)

R_μ Parameter, $R_\mu=\sqrt{r^2+\mu^2 z^2}$ (*m*)

R_μ^* Parameter, $R_\mu^*=\sqrt{r^2+\mu^2 z^2}+\mu|z|$ (*m*)

u_r/u_z Horizontal/vertical displacement of the thermoelastic medium (*m*)

α_s Linear thermal expansion coefficient of the isotropic thermoelastic medium ($°C^{-1}$)

α_{sr}/α_{sz} Linear thermal expansion coefficient of the cross-anisotropic thermoelastic medium in the horizontal/vertical direction ($°C^{-1}$)

β Thermal expansion factor of the thermoelastic medium, $\beta=(2G+3\lambda)\alpha_s$ (*Pa*/°*C*)

β_r Thermal expansion factor in the horizontal direction, $\beta_r=2G(\alpha_{sr}+\nu\alpha_{sz})/(1-2\nu)$ (*Pa*/°*C*)

β_z Thermal expansion factor in the vertical direction, $\beta_z=2G[2\nu\alpha_{sr}+(1-\nu)\alpha_{sz}]/(1-2\nu)$ (*Pa*/°*C*)

β_r^* Parameter, $\beta_r^*=2(\nu+\alpha_{sr}/\alpha_{sz})/(1-2\nu)$ (Dimensionless)

β_z^* Parameter, $\beta_z^*=2[(1-\nu)+2\nu\,\alpha_{sr}/\alpha_{sz}]/(1-2\nu)$ (Dimensionless)

$\delta(x)$ Dirac delta function (m^{-1})

ε Volume strain of the thermoelastic medium (Dimensionless)

η Parameter, $\eta=(1-\nu)/(1-2\nu)$ (Dimensionless)

ϑ Temperature increment of the thermoelastic medium (°*C*)

λ Lame constant of the isotropic thermoelastic medium (*Pa*)

λ_t Thermal conductivity of the isotropic thermoelastic medium (*J*/*sm*°*C*)

$\lambda_{tr}/\lambda_{tz}$ Thermal conductivity of the cross-anisotropic thermoelastic medium in the horizontal/vertical direction (*J*/*sm*°*C*)

ν Poisson's ratio of the isotropic thermoelastic medium (Dimensionless)

σ_{ij} Thermal stress components of the thermoelastic medium (*Pa*)

ϕ_i Functions defined in equations (11a)-(11m) (Dimensionless or m^{-1})

∇^2 Differential operator, $\nabla^2=\partial^2/\partial r^2+1/r\,\partial/\partial r+\partial^2/\partial z^2$ (m^{-2})

3-4 瞬時點熱源所引致半無限域地層之熱彈性行為的解析

ABSTRACT
Thermoelastic deformation due to an impulsive point heat source is the analog of poroelastic response caused by an impulsive point sink. In this paper, Biot's three-dimensional consolidation theory is introduced to derive the analytical solutions of the elastic transient consolidation deformation with an impulsive point sink in saturated isotropic poroelastic half space. The transient ground surface displacement produced by an impulsive point heat source is described through analog quantities between poroelasticity and thermoelasticity. Closed-form solutions of the horizontal and vertical displacements are obtained by using Laplace and Hankel integral transforms. Attention is focused on the maximum surface horizontal displacement compared to the maximum surface settlement. Results show that the horizontal displacement is about 38.5% of the maximum ground surface settlement. The study concludes that horizontal displacement is significant and should be considered in prediction of the transient settlement induced by groundwater withdrawal.

KEY WORDS
Mathematical Modelling, Transient Analysis, Point Sink, Point Heat Source

1. Introduction

Land subsidence due to groundwater withdrawal is a well-known phenomenon [1]. The pore water pressure is reduced in the withdrawal region as water pumped from an aquifer. It leads to increase in the effective stress between the soil particles and subsidence of ground surface.

The three-dimensional consolidation theory presented by Biot [2,3] is generally regarded as the fundamental theory for modeling land subsidence. Based on Biot's theory, Booker and Carter [4-7], Tarn and Lu [8] presented solutions of subsidence by a point sink in a saturated elastic half space at a constant rate. Chen [9,10], Kanok-Nukulchai and Chau [11] presented analytical solutions for the transient or steady-state responses of displacements and stresses in a half space subjected to a point sink of constant pumping rate. In the studies of Booker and Carter, the flow properties are considered as isotropic or cross-anisotropic whereas the elastic properties of the soil are treated as isotropic with pervious half space boundary. Tarn and Lu found that groundwater withdrawal from an impervious half space induces a larger amount of consolidation settlement than from a pervious one. The anisotropic permeability was proved to have significant effects on the land subsidence due to fluid extraction. Lu and Lin [12-14] displayed transient displacements of the pervious half space due to steady pumping rate [12,13] and impulsive pumping [14]. The analog between poroelasticity and thermoelasticity was discussed by Lu and Lin [12], Norris [15], Manolis and Beskos [16], *etc*. Nevertheless, the analysis of consolidation settlement and excess pore water pressure due to impulsive groundwater withdrawal corresponding with the analog between poroelasticity and thermoelasticity were not obtained in the above studies. More description on the consolidation effect due to impulsive pumping is needed in this study.

The governing equations of poro-mechanics are similar to the equations appeared in thermo-mechanics. Based on the analogy of poroelasticity and thermoelasticity, impulsive point heat source induced elastic transient horizontal and vertical displacements of the ground surface are obtained. Figure 1 shows an impulsive point sink or heat source in a stratum at a depth h where the stratum is modeled as saturated/thermally isotropic elastic half space. Point sink is usually introduced to simulate groundwater withdrawal and radioactive canister buried in a half space can be treated similar to a point heat source.

The pervious ground surface in poroelasticity is corresponding to a constant temperature of the ground surface in thermoelasticity. The elastic transient horizontal and vertical displacements of the ground surface due to an impulsive point sink, corresponding to an impulsive point heat source, are obtained by using Laplace and Hankel transforms. Results are illustrated and compared to provide better understanding of the time dependent ground surface displacements due to pumping or point heat source.

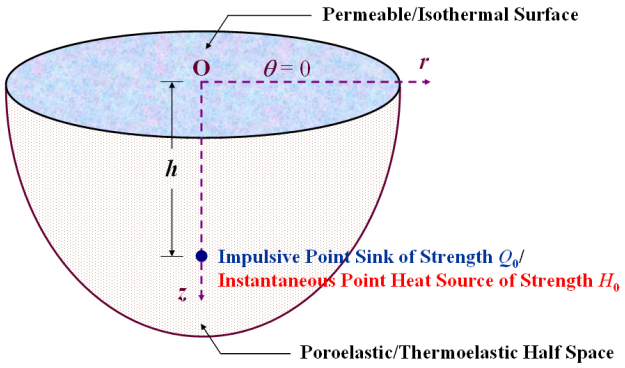

Figure 1. Impulsive point sink/instantaneous point heat source induced mechanics of poroelastic/thermoelastic problem.

2. Mathematical Model of Poroelasticity

2.1 Governing Equations

Figure 1 shows an impulsive point sink in a saturated porous stratum at a depth h. The soil mass is considered as a homogeneous isotropic porous medium. The constitutive stress behaviors of the elastic soil skeleton are

$$\sigma_{ij} = 2G\varepsilon_{ij} + \frac{2G\nu}{1-2\nu}\varepsilon_{kk}\delta_{ij} - p\delta_{ij}\ ,\ i,j = 1,2,3, \tag{1}$$

in which σ_{ij} are the total stress components; ε_{ij} are the strain components; ν is Poisson's ratio and G is shear modulus of the stratum. The excess pore water pressure p is positive for compression, and δ_{ij} is the Kronecker delta. The strains ε_{ij} and displacement components u_i are given by the linear law

$$\varepsilon_{ij} = \tfrac{1}{2}\left(u_{i,j} + u_{j,i}\right),\ i,j = 1,2,3. \tag{2}$$

The total stress must satisfy the equilibrium equations

$$\sigma_{ij,j} + b_i = 0\ ,\ i,j = 1,2,3, \tag{3}$$

where b_i denote the body forces. Eqs. (1) and (2) are used in the equilibrium equations to express their forms in displacements u_i and excess pore water pressure p as follows:

$$Gu_{i,jj} + \frac{G}{1-2\nu}\varepsilon_{kk,i} - p_{,i} = 0\ ,\ i = 1,2,3. \tag{4}$$

Consider an impulsive point sink of instantaneous strength Q_0 at time $t = 0$ located at point $(0,h)$. The uncoupled governing equation in axially symmetric coordinates (r,z) is derived from the conservation of mass and Darcy's law as

$$-\frac{k}{\gamma_w}p_{,jj} + n\beta\frac{\partial p}{\partial t} + \frac{Q_0}{2\pi r}\delta(r)\delta(z-h)\,\delta(t) = 0\,, \tag{5}$$

where k and n are the permeability and porosity of the porous medium, respectively; β is the compressibility of pore water; γ_w is the unit weight of pore water; $\delta(x)$ is the Dirac delta function. Eqs. (4) and (5) constitute the basic governing equations of the time-dependent poroelastic responses of a saturated porous medium.

2.2 Boundary Conditions and Initial Conditions

Consider the half space surface, $z = 0$, which is a traction-free and pervious boundary for all times $t \geq 0$. The mathematical statements of the boundary $z = 0$ are:

$$\sigma_{rz}(r,0,t) = 0\ ,\ \sigma_{zz}(r,0,t) = 0\ ,\text{ and }\ p(r,0,t) = 0\,. \tag{6a}$$

The boundary conditions at the remote boundary $z \to \infty$ due to the effect of an impulsive point sink must vanish at any time. This can be written as

$$\lim_{z\to\infty}\left\{u_r(r,z,t), u_z(r,z,t), p(r,z,t)\right\} = \{0,0,0\}\,. \tag{6b}$$

Assuming no initial change in displacements and seepage of the stratum, the initial conditions at time $t = 0$ of the mathematical model due to a point sink can be treated as

$$u_r(r,z,0) = 0\ ,\ u_z(r,z,0) = 0\ ,\text{ and }\ p(r,z,0) = 0\,. \tag{7}$$

The governing equations (4)-(5), correspond with the boundary conditions (6a)-(6b) and initial conditions (7) constitute the mathematical model of the presented study.

3. Mathematical Model of Thermoelasticity

3.1 Governing Equations

The constitutive behavior of the isotropic body with an instantaneous point heat source buried in a thermoelastic isotropic half space at a depth h can be expressed by

$$\sigma_{ij} = 2G\varepsilon_{ij} + \frac{2G\nu}{1-2\nu}\varepsilon_{kk}\delta_{ij} - \frac{2G(1+\nu)\alpha_s}{1-2\nu}\vartheta\delta_{ij}\ ,\ i,j = 1,2,3, \tag{8}$$

Here, σ_{ij} are the thermal stress components and ϑ is the temperature increment measured from the reference state. The constants ν, G and α_s are the Poisson's ratio, shear modulus, and linear thermal expansion coefficient of the thermoelastic medium, respectively.

The kinematic equation, Eq. (2), shows the relation between the strains and displacements, and the thermal stresses must satisfy the equilibrium relations, Eq. (3). Using Eqs. (2) and (8), the equilibrium equations (3) can be expressed in terms of displacements u_i and temperature change of the thermoelastic half space ϑ as follows:

$$Gu_{i,jj} + \frac{G}{1-2\nu}\varepsilon_{kk,i} - \frac{2G(1+\nu)\alpha_s}{1-2\nu}\vartheta_{,i} = 0\ ,\ i = 1,2,3\,. \tag{9}$$

Consider a point heat source of instantaneous point heat source of strength H_0 that is located at point $(0,h)$. The uncoupled governing equation, which is axially symmetry,

is obtained from the conservation of energy and heat conduction law as following:

$$-\lambda_t \vartheta_{,jj} + c_\varepsilon \frac{\partial \vartheta}{\partial t} - \frac{H_0}{2\pi r}\delta(r)\delta(z-h)\,\delta(t) = 0\,, \qquad (10)$$

where λ_t is the thermal conductivity and $c_\varepsilon = \rho c$. The constants ρ and c define the density and the specific heat of the thermoelastic medium, respectively. Eqs. (9) and (10) constitute the basic governing equations of the transient responses of a thermoelastic medium due to an instantaneous point heat source.

3.2 Boundary Conditions and Initial Conditions

The half space surface, z = 0, is considered as traction-free, and it does not have temperature change for all times $t \geq 0$. The boundary conditions on surface z = 0 are given by

$$\sigma_{rz}(r,0,t) = 0\,,\ \sigma_{zz}(r,0,t) = 0\,, \text{ and } \vartheta(r,0,t) = 0\,. \quad (11a)$$

The boundary conditions at the remote boundary $z \to \infty$ due to the effect of an instantaneous point heat source must vanish at any time. This can be written as

$$\lim_{z\to\infty}\left\{u_r(r,z,t), u_z(r,z,t), \vartheta(r,z,t)\right\} = \{0,0,0\}\,. \qquad (11b)$$

Assuming there are no initial change of displacement and temperature for the thermal elastic medium, the initial conditions at time $t = 0$ due to an instantaneous point heat source can be treated as

$$u_r(r,z,0) = 0\,,\ u_z(r,z,0) = 0\,, \text{ and } \vartheta(r,z,0) = 0\,. \qquad (12)$$

From these governing equations, the corresponding quantities of poroelasticity and thermoelasticity are shown in Table 1.

Table 1. Analogy of poroelastic and thermoelastic quantities.

Poroelasticity	Thermoelasticity
p	$\dfrac{2G(1+\nu)\alpha_s}{1-2\nu}\vartheta$
$n\beta$	$\dfrac{(1-2\nu)c_\varepsilon}{2G(1+\nu)\alpha_s}$
$\dfrac{k}{\gamma_w}$	$\dfrac{(1-2\nu)\lambda_t}{2G(1+\nu)\alpha_s}$
Q_0	$-H_0$

4. Analytic Solutions

Applying Laplace and Hankel integral transformations [17,18], the transient horizontal and vertical displacements of the ground surface z = 0 due to an impulsive point sink in axially symmetric coordinates (r,z) are obtained as follows:

$$u_r(r,0,t) = \frac{Q_0\gamma_w}{2(2\eta-1)\pi Gk}\left\{-\frac{cr}{\left(h^2+r^2\right)^{3/2}} + \int_0^{ct}\frac{chr}{16\tau^3}e^{-\frac{r^2+2h^2}{8\tau}}\left[I_0\left(\frac{r^2}{8\tau}\right) - I_1\left(\frac{r^2}{8\tau}\right)\right]d\tau\right\}, \quad (13a)$$

$$u_z(r,0,t) = \frac{Q_0\gamma_w}{2(2\eta-1)\pi Gk}\left\{\frac{ch}{\left(h^2+r^2\right)^{3/2}}erf\left(\frac{\sqrt{h^2+r^2}}{2\sqrt{ct}}\right) - \frac{ch}{h^2+r^2}\frac{1}{\sqrt{\pi ct}}e^{-\frac{h^2+r^2}{4ct}}\right\}, \qquad (13b)$$

where $c = k/n\beta\gamma_w$; $I_\alpha(x)$ is known as the modified Bessel function of the first kind of order α ; and $erf(x)$ denotes error function. The instantaneous ground surface horizontal and vertical displacements of the pervious half space at $t \to 0^+$ are obtained from Eqs. (13a)-(13b) as following:

$$u_r(r,0,0^+) = -\frac{cQ_0\gamma_w}{2(2\eta-1)\pi Gk}\frac{r}{\left(h^2+r^2\right)^{3/2}}\,, \qquad (14a)$$

$$u_z(r,0,0^+) = \frac{cQ_0\gamma_w}{2(2\eta-1)\pi Gk}\frac{h}{\left(h^2+r^2\right)^{3/2}}\,. \qquad (14b)$$

The maximum ground surface horizontal displacement $u_{r\,max}$ and vertical displacement $u_{z\,max}$ of the half space due to an impulsive point sink are derived from equations (14a) and (14b) by letting $r = h/\sqrt{2} \approx 0.707h$ and $r = 0$, respectively, as below:

$$u_{r\,max} = u_r\left(h/\sqrt{2}, 0, 0^+\right) = -\frac{\sqrt{3}cQ_0\gamma_w}{9(2\eta-1)\pi Gkh^2}\,, \qquad (15a)$$

$$u_{z\,max} = u_z(0,0,0^+) = \frac{cQ_0\gamma_w}{2(2\eta-1)\pi Gkh^2}\,, \qquad (15b)$$

in which the critical value $r = h/\sqrt{2}$ is derived when $du_r(r,0,0^+)/dr$ is set equal to zero. Hence, the absolute value of the displacement ratio $u_{r\,max}/u_{z\,max}$ can be derived from Eqs. (15a) and (15b) as following:

$$\left|\frac{u_{r\,max}}{u_{z\,max}}\right|\times 100\% = \frac{2\sqrt{3}}{9}\times 100\% \cong 38.5\% . \qquad (16)$$

The above result shows the maximum ground surface horizontal displacement is around 38.5% of the maximum vertical displacement for the pervious ground surface due to an impulsive point sink. Hou *et al.* [19] shown that ground surface horizontal displacement occurred when pumping from an aquifer.

The study also addressed the excess pore water pressure of the porous elastic half space due to an impulsive point sink. The transient excess pore water pressure $p(r,z,t)$ of the saturated pervious half space due to an impulsive point sink is obtained as following:

$$p(r,z,t) = \frac{Q_0\gamma_w}{8\pi k}\frac{1}{\sqrt{\pi ct^3}}\left(e^{-\frac{r^2+(z+h)^2}{4ct}} - e^{-\frac{r^2+(z-h)^2}{4ct}}\right). \qquad (17)$$

Solutions of buried point heat source induced ground surface displacements and temperature increment of the thermoelastic half space can be easily derived through the Analog parameters described in Table 1.

5. Numerical Results

The particular interest is the vertical displacement of stratum at each stage of the consolidation process, and the average consolidation ratio U is defined as:

$$U = \frac{\text{Ground surface vertical displacement at time } t}{\text{Maximum vertical displacement, } u_{z\,max}} . \qquad (18)$$

For pervious half space, U can be derived as below:

$$U = \frac{h^3}{\left(h^2+r^2\right)^{3/2}}\left[erf\left(\frac{\sqrt{h^2+r^2}}{2\sqrt{ct}}\right) - \frac{\sqrt{h^2+r^2}}{\sqrt{\pi ct}}e^{-\frac{h^2+r^2}{4ct}}\right]. \qquad (19)$$

Figure 2 shows the average consolidation ratio U at $r/h = 0$, 0.5, 1, 1.5, 2 and 10 for the impulsive pumping. Note that U initially decreases rapidly, and then the rate of vertical displacement reduces gradually. Each final value of U vanished for the saturated aquifer is treated as linear elastic porous medium in this mathematical model.

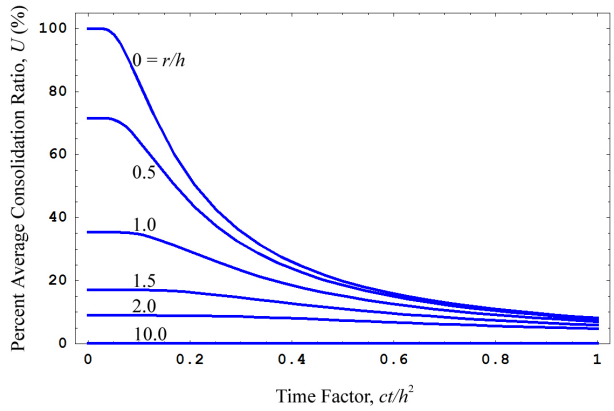

Figure 2. Average consolidation ratio U at r/h = 0, 0.5, 1, 1.5, 2 and 10 for impulsive groundwater withdrawal.

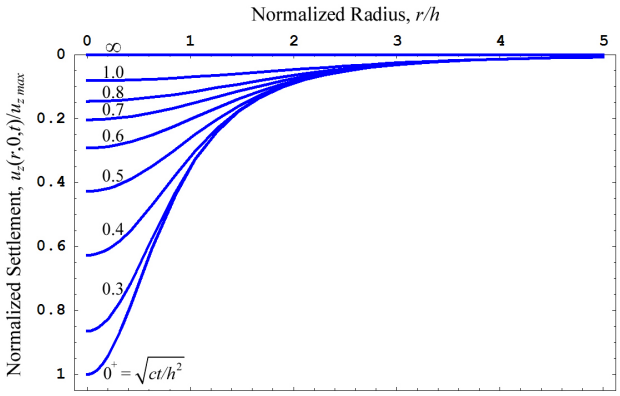

Figure 3. Normalized vertical displacement profile at the ground surface $z = 0$ for impulsive pumping.

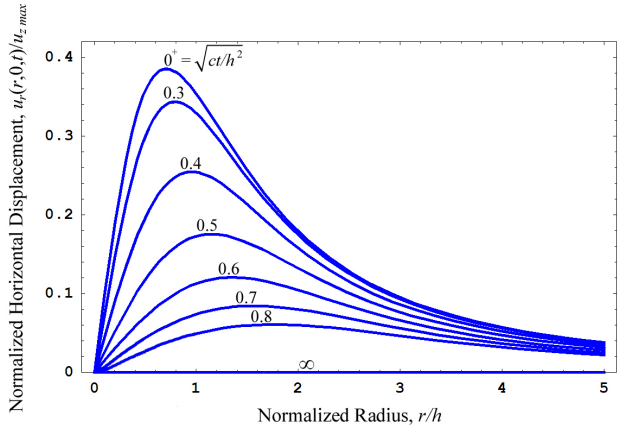

Figure 4. Normalized horizontal displacement profile at the ground surface $z = 0$ for impulsive pumping.

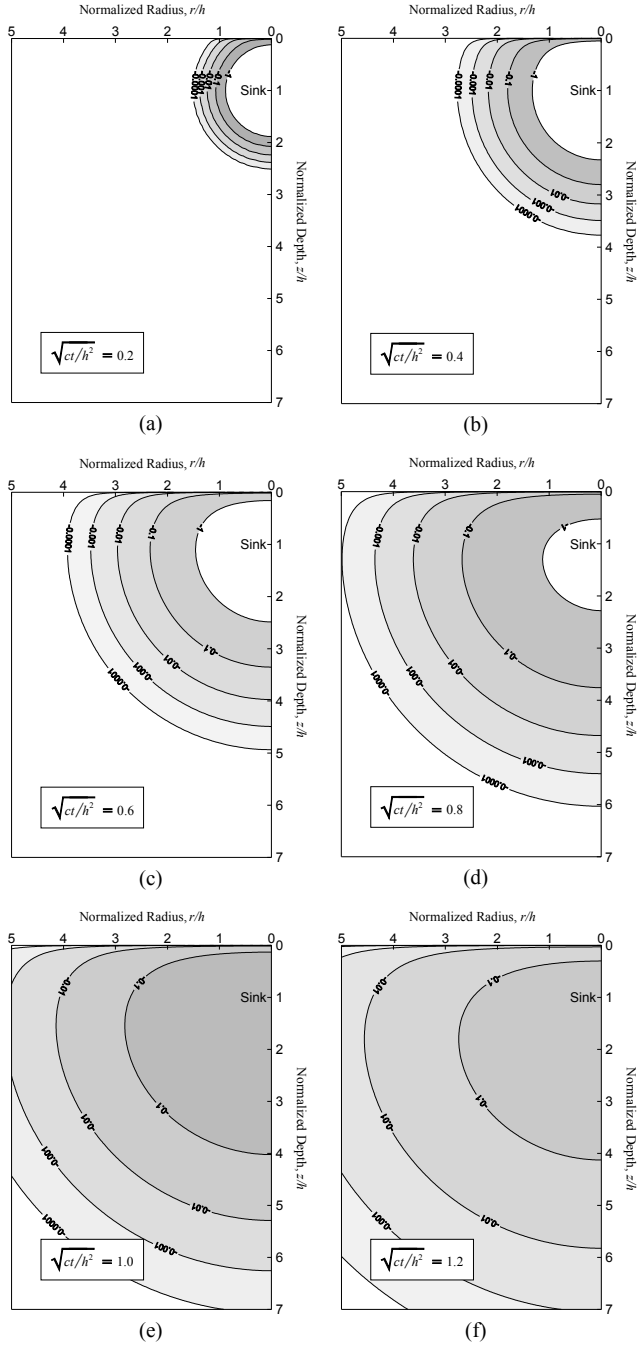

Figure 5. Distribution of normalized excess pore water pressures $p(r,z,t)/\left[cQ_0\gamma_w/8\pi^{1.5}kh^3\right]$.

The typical values for the elastic coefficients used in the practical example of the saturated medium dense sand are given in Table 2. If the pumping depth h is 10 m and the instantaneous amount of groundwater is pumped from the aquifer at Q_0 = 0.1 m^3 initially, then it has a maximum horizontal displacement and vertical displacement at the pervious ground surface of 0.88 cm and 2.28 cm, respectively.

The profiles of normalized vertical and horizontal displacements at the ground surface $z = 0$ are shown in Figures 3 and 4, respectively. The results shown in Figures 3 and 4 indicate that the ground surface displacements due to impulsive pumping can reach its extreme values initially, and then the displacements decreases gradually. Figure 4 shows that the ground surface has significant horizontal displacement, and the maximum ground surface horizontal displacement is around 38.5% of the maximum vertical displacement at $r/h \approx 0.707$ for the impulsive pumping.

From Eq. (17), the profiles of normalized excess pore water pressure $p(r,z,t)/\left[cQ_0\gamma_w/8\pi^{1.5}kh^3\right]$ of the pervious half space at four different dimensionless time factors $\sqrt{ct/h^2}$ = 0.2, 0.4, 0.6, 0.8, 1.0 and 1.2 are illustrated in Figures 5(a)-(f), respectively. The changes in excess pore water pressure have negative value p which is caused by suction of groundwater withdrawal. It's observed that the negative excess pore water pressure increases to a wider region of the aquifer initially and then gradually decreased. The impulsive pumping induced negative excess pore water pressure finally full dissipated. The elastic deformations of the stratum due to groundwater extraction will fully recover after the excess pore water pressure dissipated.

Table 2. Typical values of the elastic saturated aquifer of medium dense sand

Parameter	Symbol	Value	Units
Shear modulus [4]	G	20×10^6	N/m^2
Porosity [20]	n	0.3	–
Poisson's ratio [4]	ν	0.3	–
Permeability [4]	k	1×10^{-5}	m/s
Compressibility of water [21]	$1/\beta$	2.14×10^9	N/m^2
Unit weight of water [4]	γ_w	9,810	N/m^3

6. Conclusions

Closed-form solutions of the transient consolidation due to impulsive pumping from pervious poroelastic half space were obtained using Laplace and Hankel transformations. Vertical settlement, ground surface horizontal displacement and excess pore water pressure were investigated. The results show:

1. The corresponding quantities of poroelasticity and thermoelasticity are discussed through their governing equations. The ground surface horizontal displacement, vertical displacement and temperature increment of the thermoelastic half space due to a

buried instantaneous point heat source can be derived through their corresponding analogy listed in Table 1.

2. The ground surface displacements due to impulsive pumping reach its extreme values initially, and then the displacements decrease gradually in this model. Each final value of displacements vanished for the saturated aquifer is treated as linear elastic medium.
3. The maximum ground surface horizontal displacement is around 38.5% of the maximum vertical displacement of the pervious half space at $r = h/\sqrt{2} \approx 0.707h$. It concludes that horizontal displacement must be properly considered for better prediction of the transient consolidation deformations induced by groundwater withdrawal.

Acknowledgements

This work is supported by the National Science Council of Republic of China through grant NSC-98-2815-C-216-007-E, and also by the Chung Hua University under grant CHU-98-2815-C-216-007-E.

References

[1] J.F. Poland, *Guidebook to studies of land subsidence due to ground-water withdrawal* (Paris: Unesco, 1984).

[2] M.A. Biot, General theory of three-dimensional consolidation, *Journal of Applied Physics*, 12(2), 1941, 155-164.

[3] M.A. Biot, Theory of elasticity and consolidation for a porous anisotropic solid, *Journal of Applied Physics*, 26(2), 1955, 182-185.

[4] J.R. Booker & J.P. Carter, Analysis of a point sink embedded in a porous elastic half space, *International Journal for Numerical and Analytical Methods in Geomechanics*, 10(2), 1986, 137-150.

[5] J.R. Booker & J.P. Carter, Long term subsidence due to fluid extraction from a saturated, anisotropic, elastic soil mass, *Quarterly Journal of Mechanics and Applied Mathematics*, 39(1), 1986, 85-97.

[6] J.R. Booker & J.P. Carter, Elastic consolidation around a point sink embedded in a half-space with anisotropic permeability, *International Journal for Numerical and Analytical Methods in Geomechanics*, 11(1), 1987, 61-77.

[7] J.R. Booker & J.P. Carter, Withdrawal of a compressible pore fluid from a point sink in an isotropic elastic half space with anisotropic permeability, *International Journal of Solids and Structures*, 23(3), 1987, 369-385.

[8] J.-Q. Tarn & C.-C. Lu, Analysis of subsidence due to a point sink in an anisotropic porous elastic half space, *International Journal for Numerical and Analytical Methods in Geomechanics*, 15(8), 1991, 573-592.

[9] G.J. Chen, Analysis of pumping in multilayered and poroelastic half space, *Computers and Geotechnics*, 30(1), 2002, 1-26.

[10] G.J. Chen, Steady-state solutions of multilayered and cross-anisotropic poroelastic half-space due to a point sink, *International Journal of Geomechanics*, 5(1), 2005, 45-57.

[11] W. Kanok-Nukulchai & K.T. Chau, Point sink fundamental solutions for subsidence prediction, *Journal of Engineering Mechanics*, *ASCE*, 116(5), 1990, 1176-1182.

[12] J. C.-C. Lu & F.-T. Lin, The transient ground surface displacements due to a point sink/heat source in an elastic half-space, *Geotechnical Special Publication No. 148*, *ASCE*, 2006, 210-218.

[13] J. C.-C. Lu & F.-T. Lin, Modelling of consolidation settlement subjected to a point sink in an isotropic porous elastic half space, *Proceedings of the 17th IASTED International Conference on Applied Simulation and Modelling*, Corfu, Greece, 2008, 141-146.

[14] J. C.-C. Lu & F.-T. Lin, Analysis of transient ground surface displacements due to an impulsive point sink in an elastic half space, *Proceedings of the IASTED International Conference on Environmental Management and Engineering*, Banff, Alberta, Canada, 2009, 211-217.

[15] A. Norris, On the correspondence between poroelasticity and thermoelasticity, *Journal of Applied Physics*, 71(3), 1992, 1138-1141.

[16] G.D. Manolis & D.E. Beskos, Integral formulation and fundamental solutions of dynamic poroelasticity and thermoelasticity, *Acta Mechanica*, 76(1-2), 1989, 89-104.

[17] I.N. Sneddon, *Fourier transforms* (New York: McGraw-Hill, 1951, 48-70).

[18] A. Erdelyi, W. Magnus, F. Oberhettinger & F.G. Tricomi, *Tables of integral transforms* (New York: McGraw-Hill, 1954).

[19] C.-S. Hou, J.-C. Hu, L.-C. Shen, J.-S. Wang, C.-L. Chen, T.-C. Lai, C. Huang, Y.-R. Yang, R.-F. Chen, Y.-G. Chen, & J. Angelier, Estimation of subsidence using GPS measurements, and related hazard: the Pingtung Plain, southwestern Taiwan, *Comptes Rendus Geoscience*, 337(13), 2005, 1184-1193.

[20] K.J. Slough, E.A. Sudicky, & P.A. Forsyth, Numerical simulation of multiphase flow and phase partitioning in discretely fractured geologic media, *Journal of Contaminant Hydrology*, 40(2), 1999, 107-136.

[21] I. Vardoulakis & D.E. Beskos, Dynamic behavior of nearly saturated porous media, *Mechanics of Materials*, 5, 1986, 87-108.

Symbols

b_i	Body forces (Pa/m)
c	Parameter, $c = k/n\beta\gamma_w$ (m^2/s); Specific heat of the thermoelastic medium ($J/kg°C$)
c_ε	Parameter, $c_\varepsilon = \rho c$ ($J/m^3°C$)
$erf(x)$	Error function (Dimensionless)
G	Shear modulus of the poroelastic/thermoelastic medium (Pa)
h	Pumping depth (m); Buried depth of heat source (m)
H_0	Strength of an instantaneous point heat source (J)
$I_\nu(x)$	Modified Bessel function of the first kind of order ν (Dimensionless)
k	Permeability of the isotropic poroelastic medium (m/s)
n	Porosity of the poroelastic medium (Dimensionless)
p	Excess pore fluid pressure (Pa)
Q_0	Amount of groundwater due to impulsive pumping (m^3)
(r,θ,z)	Cylindrical coordinates system (m, *radian*, m)
t	Time (s)
u_i	Displacement components of the poroelastic/thermoelastic medium (m)
$u_{r\max}/u_{z\max}$	Maximum ground surface horizontal/vertical displacement of the poroelastic/thermoelastic medium (m)
U	Average consolidation ratio (Dimensionless)
α_s	Linear thermal expansion coefficient of the thermoelastic medium ($°C^{-1}$)
β	Compressibility of pore water (Pa^{-1})
γ_w	Unit weight of pore water (N/m^3)
$\delta(x)$	Dirac delta function (m^{-1} or s^{-1})
δ_{ij}	Kronecker delta (Dimensionless)
ε_{ij}	Strain components of the poroelastic/thermoelastic medium (Dimensionless)
ε_{kk}	Volume strain of the poroelastic/thermoelastic medium (Dimensionless)
η	Parameter, $\eta = (1-\nu)/(1-2\nu)$ (Dimensionless)
ϑ	Temperature increment of the thermoelastic medium ($°C$)
λ_t	Thermal conductivity of the thermoelastic medium ($J/sm°C$)
ν	Poisson's ratio of the poroelastic/thermoelastic medium (Dimensionless)
ρ	Density of the thermoelastic medium (kg/m^3)
σ_{ij}	Total stress components of the poroelastic medium (Pa); Thermal stress components of the thermoelastic medium (Pa)